

# Metamorphism, anatexis, zircon ages and tectonic evolution of the Gongshan block in the northern Indochina continent—An eastern extension of the Lhasa Block

Shuguang Song<sup>a,b,\*</sup>, Yaoling Niu<sup>b</sup>, Chunjing Wei<sup>a</sup>, Jianqing Ji<sup>a</sup>, Li Su<sup>c</sup>

<sup>a</sup> MOE Key Laboratory of Orogenic Belts and Crustal Evolution, School of Earth and Space Sciences, Peking University, Beijing 100871, China

<sup>b</sup> Department of Earth Sciences, Durham University, Durham DH1 3LE, UK

<sup>c</sup> Geological Lab Center, Chinese University of Geosciences, Beijing 100083, China

## ARTICLE INFO

### Article history:

Received 9 October 2009

Accepted 17 August 2010

Available online 18 September 2010

### Keywords:

Metamorphism and anatexis

Zircon dating

Crust thickening

Northern Indochina continent

Eastern Himalayan Syntaxis

Lhasa Block

Southern Tibet

## ABSTRACT

The Gongshan block near the Eastern Himalayan Syntaxis is a fault-bounded block at the northern tip of the triangle-shaped Indochina continent (NIC). Exposed in this block are late Paleozoic (Carboniferous to Permian) strata and a north–south belt of intermediate to felsic batholiths (i.e., Gaoligongshan magmatic belt). The contact between the Gaoligongshan batholiths and Carboniferous/Permian strata is characterized by a series of high-grade metamorphic gneisses with leucosome granite veins (i.e., the so-called “Gaoligong Group”). U–Pb SHRIMP and LA-ICP-MS dating of zircons indicate that these gneisses are actually metamorphosed Paleogene sediments containing inherited Archean to Cretaceous detrital zircons (from 2690 to 64 Ma) and have undergone medium- to high-pressure granulite-facies metamorphism at ~22 Ma. Leucosome and S-type granite of 22–53 Ma by anatexis are ubiquitous within high-grade metamorphic rocks in the southern part of the Gongshan block. An Early Paleozoic gneissic granite and granitoid intrusions of Jurassic, Cretaceous and Oligocene–Miocene ages are also recognized in NIC blocks. These ages suggest that the NIC differs distinctly from the Indian continent, the Greater and Lesser Himalaya zones, and the Yangtze Craton, but resembles the Lhasa Block in terms of Paleozoic to Mesozoic magmatism and detrital zircon ages. This offers an entirely new perspective on the tectonic evolution of the Gongshan block in particular and of the history of the Lhasa Block in the context of the India–Asia continental collision in general. Furthermore, the high-grade metamorphism in the NIC indicates a strong crustal thickening (vs. strike-slip shearing) event during much of the Eocene to the Oligocene (~53–22 Ma) that has brought the Paleogene sediments to depths of greater than 25 km. Continuous northward convergence/compression of the Indian Plate at the Eastern Himalayan Syntaxis may have led to the clockwise rotation, southeastward extrusion and extension of the southeastern part of the Indochina continent.

© 2010 Elsevier B.V. All rights reserved.

## 1. Introduction

From the Eastern Himalayan Syntaxis to the southeast is a triangular region bordered by the Ailaoshan–Red River left-lateral strike-slip fault to the east, by the Sagaing right-lateral fault to the west, and by the Puqu fault, the southeast branch of the Jiali fault zone (Lee et al., 2003), at the northern tip. This region has been defined as “Indochina continent” (e.g. Tapponnier et al., 1986; Replumaz and Tapponnier, 2003) and has been interpreted as a zone of tectonic escape resulting from the India–Asian continental collision and continued convergence in the Cenozoic (Tapponnier et al., 1986; Peltzer and Tapponnier, 1988; Holt et al., 1991). Associated with the escaping are many geological features in the region, including a clockwise flow of materials at the northeastern edge of India. Both the

geology and recent tectonic histories recorded in the Indochina continent, therefore, are critical towards a genuine understanding of the deformation processes of the Tibetan Plateau and its peripheral regions in response to the India–Asia continental collision.

Previous studies in this region have mainly focused on the initiation, histories and kinematics of the complex strike-slip fault systems (e.g., Tapponnier et al, 1990; Wang and Burchfiel, 1997; Ji et al., 2000a; Socquet and Pubellier, 2005; Searle, 2006). However, the nature and history of crustal materials of the northern Indochina continent (NIC) as well as its relationships with the rest of the continent and with the adjacent tectonic terranes (i.e., the Yangtze Craton to the east, the Indian continent and Himalayan–Tibetan orogenic belt to the west) remain unclear. Furthermore, the nature and magnitude of the displacement associated with the tectonic escaping (e.g., rotational thickening vs. lateral extrusion) are still in debate (England and Molnar, 1990, 1997, 2005; Tapponnier et al, 1990, 2001; Houseman and England, 1993; Burchfiel and Wang, 2003).

In this paper, we present new data on representative metamorphic and magmatic rocks from the Gongshan block in the NIC. These

\* Correspondent author. MOE Key Laboratory of Orogenic Belts and Crustal Evolution, School of Earth and Space Sciences, Peking University, Beijing 100871, China. Tel.: +86 10 62767729; fax: +86 10 62751159.

E-mail address: [sgsong@pku.edu.cn](mailto:sgsong@pku.edu.cn) (S. Song).

include granulite-facies metapelites from the Gaoligong Group and granitoid samples in the southern Gongshan block. The data include cathodoluminescence (CL) imaging, sensitive high-resolution ion microprobe (SHRIMP II) and laser ablation (LA) ICP-MS analyses to determine the ages of detrital, magmatic and metamorphic zircons. We use these data to deduce the provenance of protolith sediments and crustal affinity with the Himalaya and Lhasa Terranes in southern Tibet, and then discuss the tectonic evolution of the NIC in response to the India-Asia continental collision.

## 2. Geological background

### 2.1. Tectonic units of the NIC

The NIC, which is southeast of the Eastern Himalayan Syntaxis, is tectonically active with three major rivers (Jinshajiang, Lanchang-

jiang, and Nujiang) running in a narrow region. The crust here is strongly shortened with varying degrees of deformation as a result of the bulldozer-like northeastward compression of the eastern Indian continent. The NIC has been divided into four sub-blocks: the Gongshan (GB), Baoshan (BB), Tengchong (TB) and Lanping-Simao (LB) blocks (Fig. 1b) (e.g., Zhong, 1998; Wang et al., 2006). The first three blocks are thought to have the same crustal architecture and basement on the basis of similar Paleozoic strata and high-grade metamorphism (YBGM, 1990; Zhong, 1998). All these four blocks are bounded by Cenozoic faults with complex histories of ductile and brittle deformation.

#### 2.1.1. Tengchong block (TB)

The Tengchong block (Fig. 1b) is the northern continuation of the Mogok metamorphic belt of Myanmar (Mitchell, 1989; Bertrand et al., 1999, 2001). In Myanmar, it is bounded by the dextral Sagaing fault to

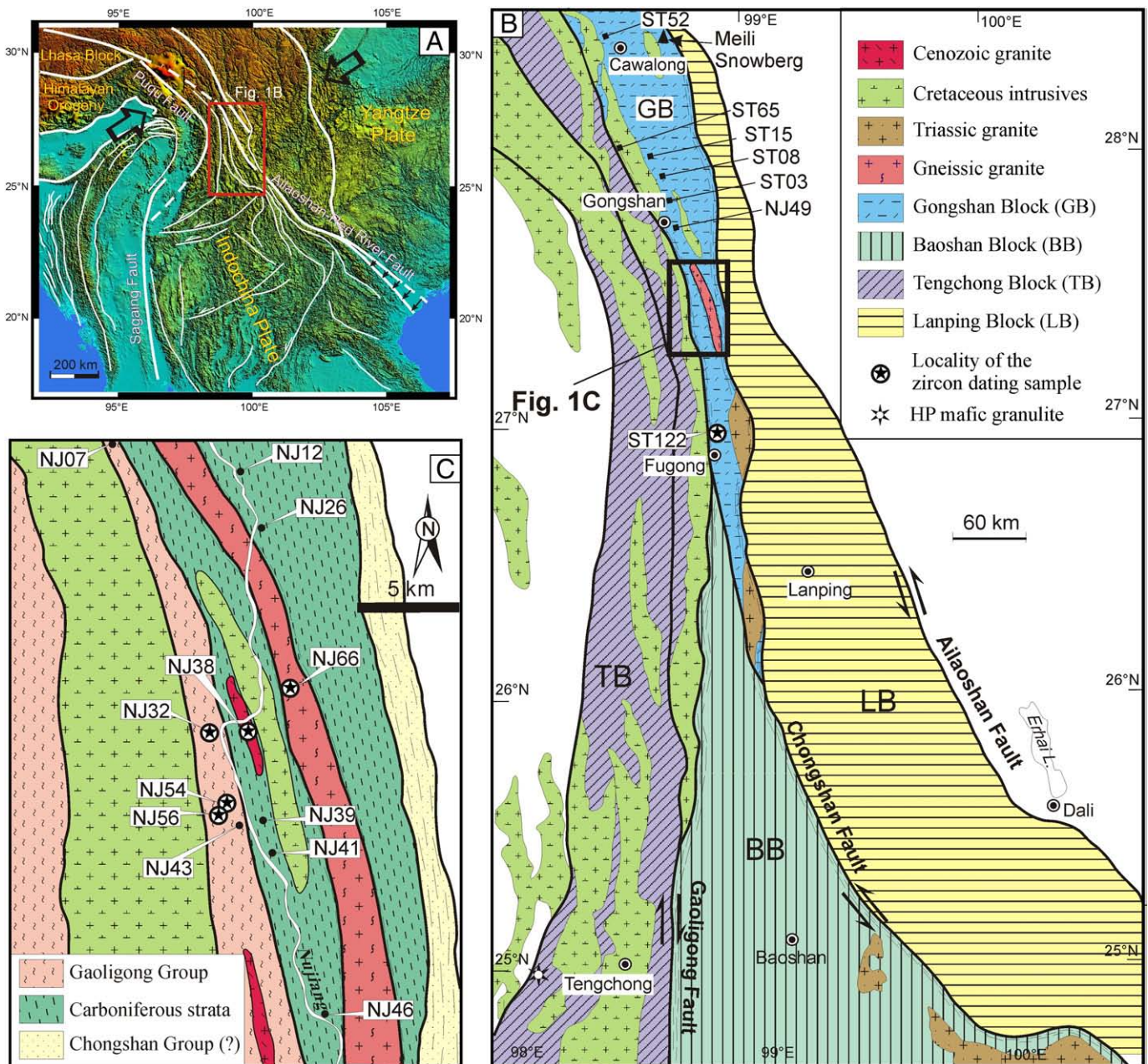


**Fig. 1.** (a) Tectonic framework of the Southeast Asia subcontinent (modified from Tapponnier et al., 2001; Socquet and Pubellier, 2005). (b) Simplified geological map of the northern Indochina continent (NIC) showing its tectonic units (modified after YBGM, 1990; Pana and Ding, 2004). (c) Geological map of the study area with sample locations. All units except granite are amphibolite to granulite facies metamorphic rocks.

the west and by the Gaoligong shear zone to the east. It has been considered as part of Gondwana during the late Paleozoic and was accreted to Eurasia in the late Mesozoic (Wang, 1983; Morley et al., 2001). The block is mainly composed of high-grade metamorphic complexes, low- to medium-grade metamorphosed Paleozoic strata, Mesozoic–Tertiary granites and Tertiary–Quaternary volcanic–sedimentary sequences (YBGMR, 1990). Medium to high-pressure mafic granulite has been reported in the China–Myanmar border (see Fig. 1b for locality; Ji et al., 2000a,b) with an assemblage of garnet + clinopyroxene + plagioclase + amphibole + quartz and metamorphic conditions of  $P=8\text{--}10$  kbar and  $T=750\text{--}860$  °C. Amphibole and plagioclase Ar–Ar dating gives plateau ages of 23–24 Ma. The Paleozoic strata are mainly composed of weakly metamorphosed sandstones, shale/slate and limestone with cold-water fossil species (Wang, 1983).

### 2.1.2. Baoshan block (BB)

The Baoshan block (Fig. 1b) in the south is wedge-shaped and bounded by the Gaoligong shear zone to the west and by the Chongshan shear zone to the east (e.g., Zhang et al., 2010). Rock types in the block, as described in YBGMR (1990), include a high-grade metamorphic complex (Gaoligong Group?), low- to medium-grade metamorphosed Paleozoic strata, Mesozoic–Tertiary granites and Tertiary–Quaternary sediments, similar to the Tengchong block. A comparison of sedimentary facies and fossils in the Carboniferous and Permian strata has led to the suggestion that the Tengchong and Baoshan blocks both may in fact be a fragment from Gondwana (Wang, 1983). Zhong (1998) suggested that the block was amalgamated with the Yangtze Craton along the Changning–Menglian suture zone in Late Paleozoic time.

### 2.1.3. Lanping–Simao block (LB)

The Lanping–Simao block (or fold belt) is bounded by Ailaoshan shear zone to the east and by Chongshan shear zone to the west. The block shows outcrops of Proterozoic basement and has Paleozoic marine strata that might be similar to those of the Yangtze Block (Wang et al., 2006). The late Paleozoic strata are mostly thick basaltic to felsic volcanic sequences and terrigenous turbidites deposited in a forearc basin of an active continental margin (Zhong, 1998). Thick Triassic continental sediments are mainly exposed along the southwestern margin of the belt (Zhong, 1998; Peng et al., 2006) and rest unconformably on pre-Mesozoic strata.

### 2.1.4. Gongshan block (GB)

The Gongshan block in this paper refers an elongated massif in the northern termination of the NIC. The block is bounded by the Chongshan shear zone to the east and by the Gaoligong shear zone to the west (Fig. 1). It may link to the Baoshan block in the south; to the north, it gradually changes its strike to NW–SE around the Eastern Himalayan Syntaxis. It is so far unclear if this block is tectonically related to the Lhasa block in southern Tibet. The block mainly consists of the Late Paleozoic (Carboniferous to Permian) sedimentary strata with varying grade of metamorphism (see below). A high-grade metamorphic complex, i.e., the Gaoligong Group, occurs as an N–S belt in the southern Gongshan block. This group consists of metapelite, migmatitic gneisses and leucogranite and has long been thought as the Precambrian basement of the NIC (Zhai et al., 1990; Zhong, 1998; Wang et al., 2006). The sedimentary assemblage includes sandstones with layers of glacial conglomerate, siltstone, shale and marble. The fossil records in the low-grade metamorphic layers suggest that the Late Paleozoic strata represent the Gondwana type of littoral to continental shelf sediments, as are those in the Tengchong and Baoshan blocks (YBGMR, 1990). The Upper Paleozoic strata in the Gongshan block consist of metamorphosed sandstone, siltstone, mudstone, marble and basaltic layers of greenschist- to granulite-facies. These metamorphic strata are strongly deformed and intruded

by sheet-like granitoid plutons of varying size and garnet-bearing leucogranite veins. One garnet-bearing (S-type) gneissic pluton occurs as an elongated block (~2–4 km wide and ~50 km long) in shear contact with the host Paleozoic strata (Fig. 1c). Along the Gaoligongshan mountain range is an N–S belt of Cretaceous intrusions, i.e., the Gaoligongshan magmatic belt (Fig. 1b) with varying zircon U–Pb ages of 70–140 Ma (Yan et al., 2002; Chen et al., 2006). Triassic granites with zircon U–Pb ages of 200–259 Ma and Early Paleozoic granitic gneiss (490-Ma S-type granite) have also been reported from both Gongshan and Baoshan blocks (YBGMR, 1990; Peng et al., 2006; Song et al., 2007) (Fig. 1b).

The right-slip Gaoligong shear zone is marked by a series of mylonite zones located between the Gongshan and Tengchong Blocks in the north and between the Baoshan and Tengchong Blocks in the south (Fig. 1b). This shear zone, together with the right-slip Sagaing fault (Fig. 1a) to its southwest, has been considered to be a conjugate shear system to the left-slip Ailao Shan shear zone (Wang and Burchfiel, 1997; Ji et al., 2000a; Yin and Harrison, 2000; Socquet and Pubellier, 2005). However, the dextral Sagaing fault, i.e., the west boundary of the Indochina continent, was not active prior to 15 Ma (Morley et al., 2001; Replumaz and Tapponnier, 2003). The total displacement of ~700 km (Replumaz and Tapponnier, 2003) along the Sagaing fault, if correct, would suggest that the extrusion (i.e., the escape) of the Indochina continent has been rather rapid in the past 15 million years.

## 2.2. Metamorphic architecture in the Gongshan block

The Gongshan block exhibits spatial variation in metamorphic grade. In the north segment (north of Cawalong, see Fig. 1b for location), all the rocks (except for granite intrusions) show amphibolite-facies metamorphism, e.g., marble of Carboniferous limestone, garnet-staurolite-mica schist of mudstone (Fig. 2a), and amphibolite of basaltic layers. The early minerals of garnet, staurolite and biotite as porphyroblasts have been strongly overprinted and foliated by the late muscovite + albite + quartz assemblage that is genetically associated with the strike-slip shearing (Fig. 2b). In the middle segment of the Gongshan block (from Cawalong to north of Gongshan), sandstone, siltstone, mudstone, limestone and basalts of Carboniferous to Permian age have undergone sub-greenschist to greenschist-facies metamorphism (Fig. 2c–f). The common metamorphic assemblage of the strongly deformed mylonite consists of fine-grained white mica, calcite and chlorite with rare biotite (Fig. 2h and g). In the southern segment of the Gongshan block (our primary study area), the metamorphic grade increased from lower amphibolite to upper amphibolite and to granulite facies (see below). All these observations reflect the varying depths of erosion in response to differential tectonism in the N–S direction.

## 3. Petrography and metamorphism of the southern Gongshan block

The southern segment of the Gongshan block (Gongshan-Fugong region, see Fig. 1b for location) includes (1) metamorphosed Carboniferous strata and (2) the Gaoligong Group. Two events of metamorphism can be recognized. The earlier event is pervasive varying, from north to south, in conditions from amphibolite to granulite facies with localized anatexis. The later event is restricted to narrow and strongly deformed shear zones, overprinting the early fabrics and cutting Gaoligongshan granitoid plutons.

### 3.1. Metamorphism and deformation of the Carboniferous strata

The Carboniferous strata of sandstone, limestone, mudstone and basaltic layers have all undergone varying grade of metamorphism, comparable to the metamorphosed Carboniferous strata in the north.

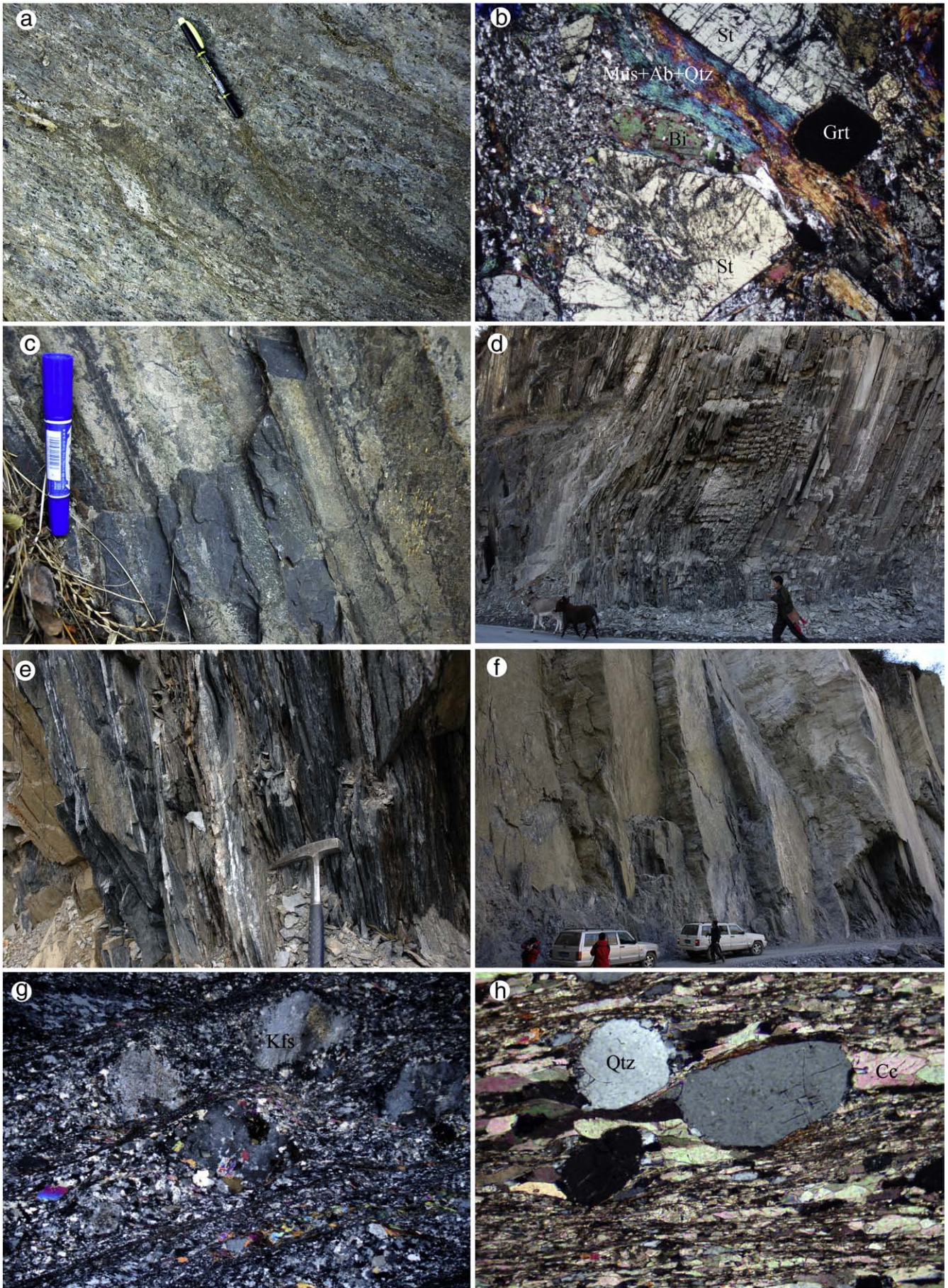


**Table 1**  
Mineral assemblage and *P–T* estimates of meta-pelites from the southern Gongshan block.

Samples	Group	Mineral assemblage	THERMOCALC 3.23 average <i>P–T</i> (Powell et al., 1998)	gt-bi thermometry (Holdaway 2000)
ST56	Carboniferous	gt, bi, st, pl, mu, q, ilm, tour, ap	$T = 648\text{ }^{\circ}\text{C}$ , $sd = 58$ , $P = 7\text{ kbar}$ , $sd = 2.1$ $\sigma_{fit} = 2.09$	635 °C (6 kbar)
NJ49	Carboniferous	gt, bi, st, ky, pl, mu, q, ilm, tour, ap	$T = 650\text{ }^{\circ}\text{C}$ , $sd = 21$ , $P = 8.3\text{ kbar}$ , $sd = 1.4$ $\sigma_{fit} = 1.34$	622 °C (6 kbar)
NJ12	Carboniferous	gt, bi, sil, ksp, pl, mu, q, ilm, tour, ap	$T = 685\text{ }^{\circ}\text{C}$ , $sd = 60$ $P = 6.5\text{ kbar}$ , $sd = 1.4$ $\sigma_{fit} = 1.14$	679 °C (6 kbar)
NJ39	Carboniferous	gt, bi, sil, pl, ksp, mu, q, ilm, tour, ap	$T = 711\text{ }^{\circ}\text{C}$ , $sd = 28$ $P = 6.7\text{ kbar}$ , $sd = 1.2$ $\sigma_{fit} = 1.05$	737 °C (6 kbar)
NJ07	Gaoligong Group	gt, bi, sil, ky, pl, ksp, mu, q, ilm, tour, ap	$T = 734\text{ }^{\circ}\text{C}$ , $sd = 18$ $P = 8.4\text{ kbar}$ , $sd = 0.5$ $\sigma_{fit} = 1.71$	689 °C (6 kbar)
NJ32	Gaoligong Group	gt, bi, sil, pl, ksp, mu, q, ilm, tour, ap	$T = 684\text{ }^{\circ}\text{C}$ , $sd = 32$ $P = 6.7\text{ kbar}$ , $sd = 2.0$ $\sigma_{fit} = 1.55$	631 °C (6 kbar)
NJ43	Gaoligong Group	gt, bi, sil, pl, per, mu, q, ilm, ap	$T = 746\text{ }^{\circ}\text{C}$ , $sd = 53$ $P = 6.8\text{ kbar}$ , $sd = 2.1$ $\sigma_{fit} = 1.66$	737 °C (6 kbar)
NJ54	Gaoligong Group	gt, bi, sil, pl, ksp, mu, q, ilm, tour, ap	$T = 725\text{ }^{\circ}\text{C}$ , $sd = 11$ $P = 7.1\text{ kbar}$ , $sd = 2.6$ $\sigma_{fit} = 2.34$	711 °C (6 kbar)

See Fig. 1 for sample locations. Mineral abbreviations: ab, albite; bi, biotite; cd, cordierite; chl, chlorite; ctd, chloritoid; gt, garnet; ky, kyanite; ksp, K-feldspar; pa, paragonite; mu, muscovite; per, perthite; pl, plagioclase; q, quartz; sill, sillimanite; st, staurolite.

### 3.1.1. Metapelite

Metapelite in the northern part of the southern Gongshan block is coarse-grained with a mineral assemblage of gt + st + ky + bi + mu + pl + q (see Table 1 for mineral abbreviations) (Fig. 3a and b) plus accessory minerals (e.g., ilmenite, tourmaline, apatite, zircon and monazite). Towards the south, the mineral assemblage changes into gt + sill + bi + ksp + pl + q + ilm through the reaction of muscovite + quartz = K-feldspar + Al<sub>2</sub>SiO<sub>5</sub> + H<sub>2</sub>O. Further to the south, perthite appears in the assemblage along with garnet and sillimanite, but biotite modal content decreases and garnet-bearing leucogranite pods or veins become common within the strata (Fig. 3c), suggesting that anatexis must have taken place in the metapelite under granulite-facies conditions. The late greenschist facies metamorphism (i.e., an assemblage of fine-grained muscovite, albite, chlorite and quartz) was associated with shear deformation, strongly overprinting the peak assemblages (Fig. 3a and b).

### 3.1.2. Calcic sandstone

Calcic sandstone is one of the major rock types of the Carboniferous strata interlayered with metapelite and marble. The rock shows a medium- to fine-grained granular texture with a metamorphic mineral assemblage of diopside + biotite + quartz ± calcite ± amphibole. With increasing metamorphic grade from north to south, amphibole content decreases. A diopside + scapolite assemblage has been observed in some samples in the south (Fig. 3d). Retrograde assemblage of amphibole + epidote (+ chlorite) is present in most samples.

### 3.1.3. Marble

Marble interlayers can be traced steadily following the strata from north to south. In the northern part of the southern Gongshan block, marbles are mostly pure with coarse-grained calcite and minor diopside. Garnet-clinopyroxene layers and pods exist within the marble and show a medium-grained granular texture without strong deformation (Fig. 3e). The garnet is CaO rich with high grossular (70.5 mol%), low almandine (28.5 mol%) and extremely low pyrope (0.25 mol%). The clinopyroxene is diopside with high wollastonite (~49.5–50 mol%), and low ferrosilite (~19.7–21.8 mol%) and enstatite (~28.1–30.8 mol%). In the southern part of the southern Gongshan block, marble is coarse-grained with a granoblastic texture and consists of phlogopite + diopside + calcite + olivine ± quartz (Fig. 3f). Mg<sup>#</sup> (Mg/[Mg + Fe]) of diopside in the marble gradually increases from north to south. The mineral assemblage and composition suggest an increase in metamorphic temperatures from north to south.

### 3.1.4. Deformation of the late Paleozoic strata

The style and intensity of deformation also vary from north to south as manifested by the behavior of calcic meta-sandstone layers. In the conjunct region between the middle and southern segments of the Gongshan block, metamorphism is under greenschist and lower-amphibolite facies conditions, deformation of the Carboniferous sandstone/siltstone is characterized by isoclinal folds with high-angle axial planes (Fig. 4a and b). With increasing metamorphic grade towards south, sedimentary layers are replaced by axial schistosity (Fig. 4c and d) before they disappear completely (Fig. 4e) in the southern segment. These deformations are mostly associated with E–W lateral compression and vertical thrust.

### 3.2. Petrography and metamorphism of the Gaoligong Group

In the literature, the “Gaoligong Group” is referred to the high-grade metamorphic complex exposed in the NIC blocks (i.e., the Tengchong, Baoshan and Gongshan blocks) (e.g., YBGMR, 1990; Zhong, 1998). This group has long been described as the Precambrian basement of the NIC because of the high-grade metamorphism (Zhai et al., 1990; Zhong, 1998; Wang et al., 2006). In our study area, the Gaoligong Group mainly crops out along both sides of the Gaoligong shear zone in the southern Gongshan block. It consists of high-grade pelitic gneiss, migmatite and abundant garnet-bearing leucogranite pods/veins (see below).

Pelitic gneisses from the Gaoligong Group (samples NJ32, NJ54 and NJ56, Fig. 1c) contain a mineral assemblage of gt + sil + ksp + bi + pl + q (+ ilm + tour + zir + mon) (Fig. 5a). Muscovite is an unstable phase and occurs as relics of the reaction: gt + mu + pl = bi + ksp + Al<sub>2</sub>SiO<sub>5</sub> + melt during anatexis (Fig. 5b and c). Perthite appears both in some pelitic gneisses and in the leucogranite (Fig. 5d). Kyanite is observed in some samples coexisting with garnet, sillimanite, K-feldspar and biotite (Samples NJ07, Fig. 5e), suggesting medium- to high-pressure metamorphism along the kyanite-sillimanite phase boundary.

### 3.3. Strike-slip shearing deformation in the Gongshan block

Strike-slip shear zones are well developed in our study area and have been previously described as “the Gaoligong fault system” (see Wang and Burchfiel, 1997; Socquet and Pubellier, 2005). These shear zones trend N–S in the south and turn gradually to NW towards north. They cut through the high-grade metamorphic rocks of the Gaoligong Group, granitoid plutons and Carboniferous strata. Mylonites in the

**Fig. 2.** Photographs showing rocks from the middle and northern segments of the Gongshan block. (a) Garnet-staurolite schist north of Cawalong (sample location of ST52 in Fig. 1b). (b) Microfabrics of ST52 showing garnet (Grt) + staurolite (St) + biotite (Bi) with the overprint of foliated muscovite (Mus) + albite (Ab) + quartz (Qtz). (c) Low-grade metamorphosed Carboniferous sandstone north of Gongshan (sample location of ST03). (d) Carboniferous slate in the middle of the Gongshan (sample location of ST15). (e) Low-grade, strongly deformed limestone + siltstone in the northern part of the Gaoligong shearing zone in the middle of the Gaoshan block (sample location of ST08). (f) Very low-grade metamorphosed sandstone with near-horizontal shearing lineations in the middle of the Gongshan block. (g) Microfabrics of mylonized granite with newly-formed muscovite along foliations in the northern part of the Gaoligong shearing zone in the middle of the Gongshan block (ST65). (h) Mylonized marble with muscovite + chlorite along foliations in the northern part of the Gaoligong shearing zone (ST08).

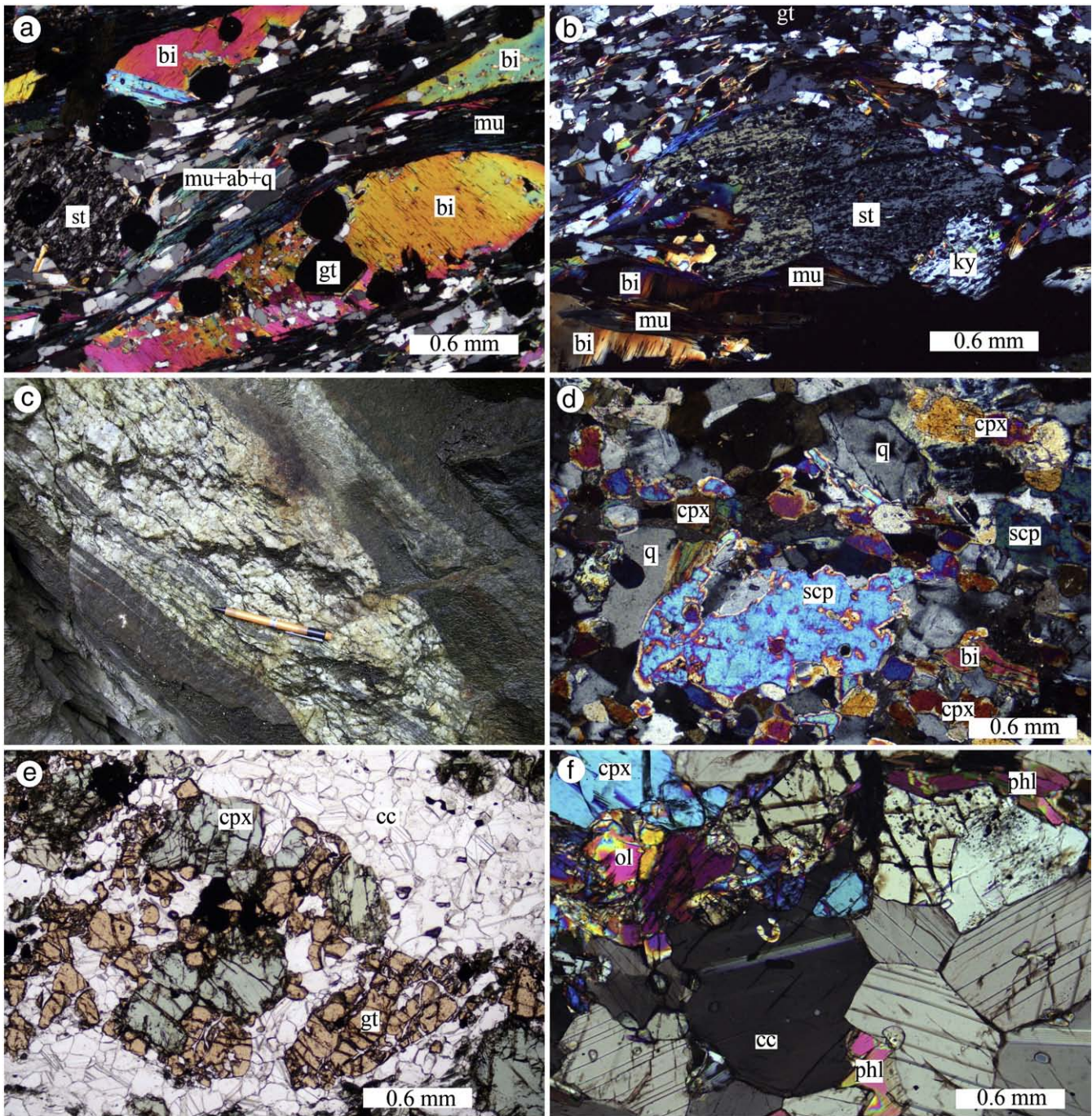


**Fig. 3.** Photographs of rocks from the metamorphosed Carboniferous strata in the southern Gongshan block. (a and b) Metapelite showing that the early amphibolite-facies assemblage of  $gt + bi + st + ky$  is overprinted by mylonite foliation with  $mu + ab + q$  (greenschist-facies) assemblage (NJ49); K–Ar dating of muscovite gives mylonitization age of  $10.1 \pm 0.8$  Ma. (c)  $gt$ - $mu$ -bearing leucogranite vein in the metamorphosed Carboniferous sandstone (location near NJ39). (d) High-grade meta-sandstone with  $cpx$  (clinopyroxene) +  $scp$  (scapolite) +  $pl + bi + q$  assemblage (NJ46). (e)  $gt + cpx$  assemblage within marble (NJ26). (f) High-grade marble with  $ol$  (olivine) +  $cpx + phl$  (phlogopite) +  $cc$  (calcite) (NJ41).

shear zones consist of low-grade greenschist facies minerals of muscovite + chlorite + albite, which overprint the early amphibolite to granulite facies assemblages (Fig. 5d). Ar–Ar dating of amphibole, biotite and muscovite gave inconsistent ages from 24 to 12 Ma (Wang and Burchfiel, 1997; Ji et al., 2000a,b).

#### 4. Anatexis in the Gongshan block

Garnet-bearing leucosome and S-type granite are widespread as small lenses and veins of varying size within both high-grade metamorphosed “Carboniferous strata” and “Gaoligong Group”. These

anatectic granites include garnet-muscovite granite, fine-grained garnet-bearing biotite-muscovite granite and tourmaline granite.

Field observations suggest that leucogranite (garnet-muscovite granite) is internally derived. Fig. 6 displays snapshots of the processes of leucogranite generation through partial melting (anatexis) of metapelite. Melts produced from the metapelite are extracted (Fig. 6a) as pockets or veins with varying thickness (~5 to 80 cm; Fig. 6b and c). Foliations inherited from the metapelite can also be locally preserved in leucogranite pockets (Fig. 6d). Some leucosome occurs as veins intruding the Carboniferous marble and sandstone layers, and cut the schistosity of their country rocks (Fig. 6e and f). Most of the leucogranite shows a medium- to coarse-

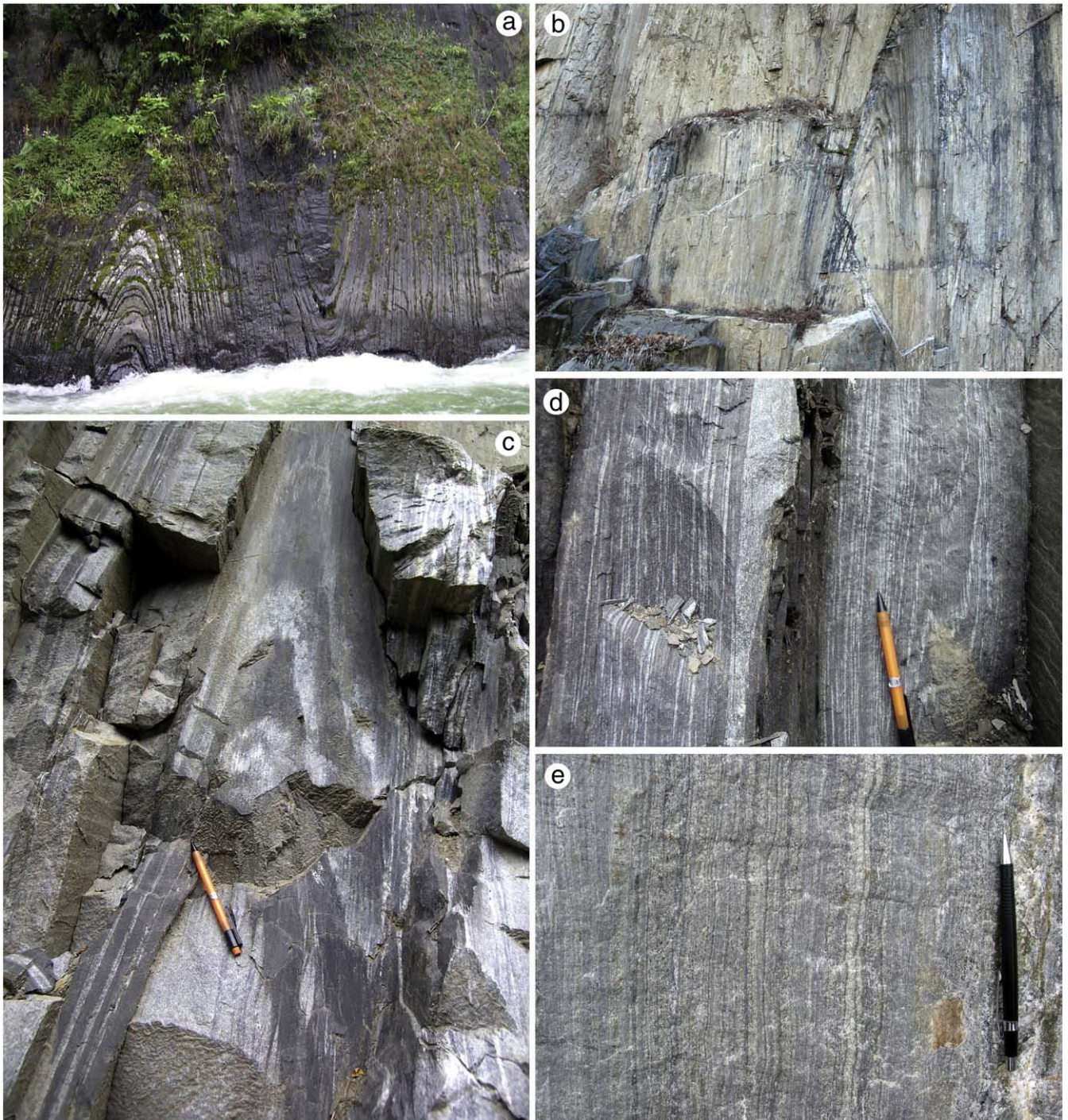


**Fig. 4.** Photographs showing deformation of metamorphosed Carboniferous sandstone layers. (a) and (b) Tight to isoclinal folds with near-vertical axial-plane in metamorphosed sandstone and slate near Gongshan. (c) Isoclinal fold with near-vertical axial-plane schistosity in the amphibolite-facies meta-sandstone. (d) Sedimentary beddings are strongly replaced by near-vertical axial-plane schistosity. (e) Sedimentary beddings are totally replaced by the axial-plane schistosity in high-grade meta-sandstone. From (a) to (e), metamorphic grade gradually increases.

grained granoblastic texture with weak foliation. The mineral assemblage includes varying modal content of garnet, muscovite, plagioclase, perthite and quartz with or without sillimanite, which represent the product of anatexis during high-grade metamorphism. Most leucosome and S-type granite are weakly deformed and are petrogenetically unrelated to the lateral shear deformation.

Fine-grained garnet-bearing biotite-muscovite granite (sample NJ38, Fig. 1c) occurs as lenses with the long axis parallel to the tectonic trend. Contacts between the granite and meta-sandstone are unclear because of the tectonic juxtaposition and shear deformation. The granite

consists of quartz (30–35%), plagioclase (20–25%), K-feldspar (~35%), biotite (5–8%), muscovite (2–3%) and minor garnet (<1%).

The tourmaline granite (samples ST122 and NJ74) occurs as small sheet-like bodies of 30–50 m<sup>2</sup> in size within the metamorphosed Carboniferous strata (see the locality in Fig. 1b). It is fine- to medium-grained with an assemblage of quartz (30–35%), plagioclase (25–30%), K-feldspar (30–35%), tourmaline (~5–8%) and minor garnet and white mica. The mineral assemblage and whole-rock composition suggest that the tourmaline granite is also a peraluminous (or S-type) granite of anatectic origin.

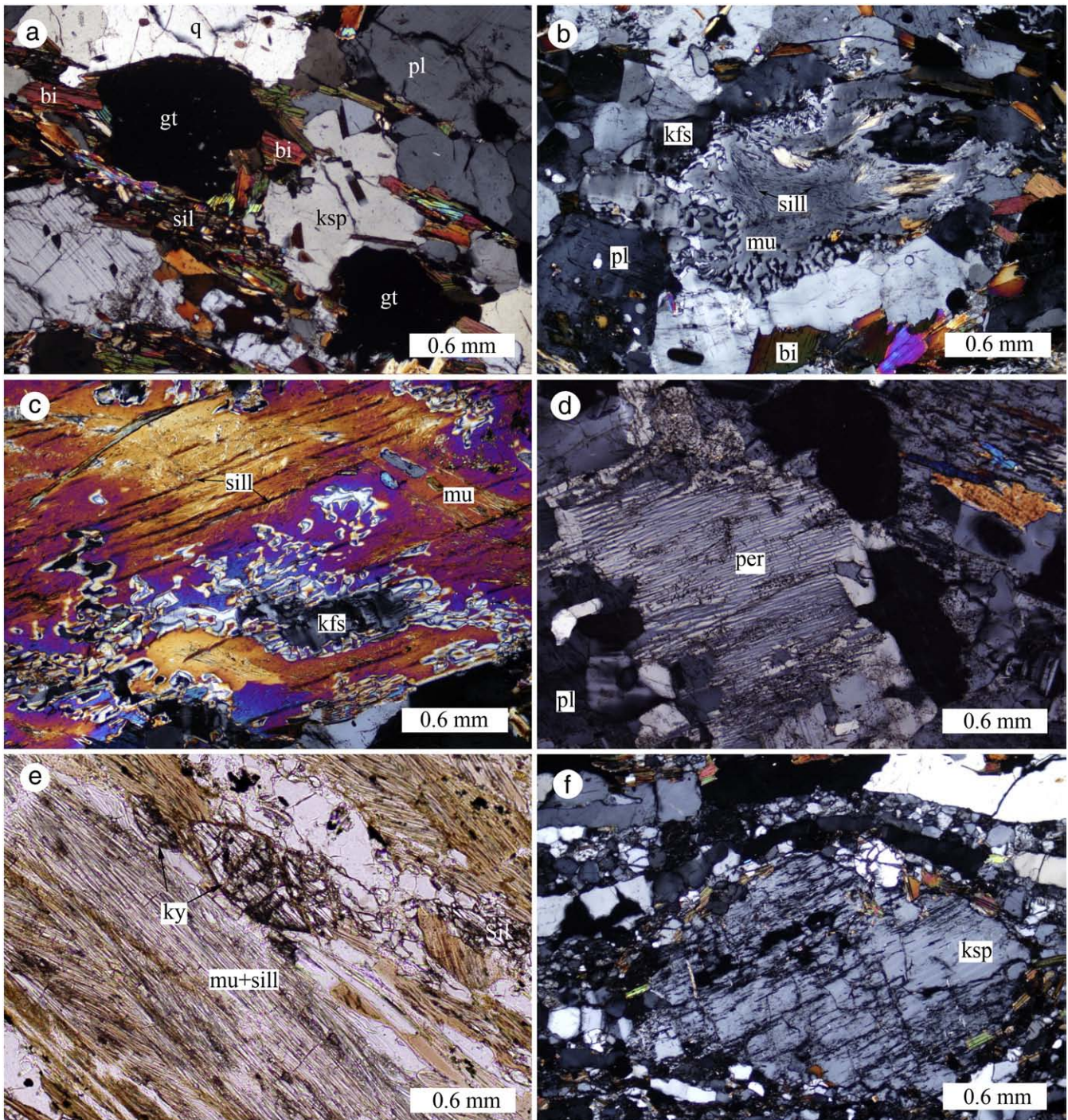


**Fig. 5.** Photomicrographs showing texture and mineral assemblage of the high-grade metapelite. (a) Texture of pelitic gneiss with  $gt + bi + pl + ksp + sill + q$  (NJ54). (b and c) Reacted textures showing relic muscovite and newly-formed K-feldspar and sillimanite through the reaction of  $mu + q = ksp + sill + H_2O$ . (d) Perthite in muscovite-bearing leucogranite (NJ44). (e) Relic kyanite + biotite (+ garnet) assemblage replaced by late needle-shaped sillimanite + muscovite (NJ07). (f) Relic K-feldspar (kfs) in a mylonitized pelitic gneiss with secondary low-grade mylonite assemblage of  $mu + al + q (+ chl)$  (NJ56).

## 5. Mineral chemistry and *P-T* estimates

Mineral compositions were analyzed using a JEOL JXA-8100 EPMA (electron probe micro-analyzer) at Peking University. The operation conditions are 15 kV acceleration voltage, 10 nA beam current and 2  $\mu$ m spot size. Synthetic silica (Si), spessartine (Mn) and  $Cr_2O_3$  (Cr), natural sanidine (K), pyrope (Mg), andradite (Fe, Ca), albite (Na, Al) and rutile (Ti) as well as relevant standard minerals (from SPI corp. US) were used as calibration standards for relevant elements given in

parentheses. Representative analyses for various minerals and garnet compositional profiles are given in Appendix A (Tables A1–A7).

### 5.1. Compositional variation of garnet

Garnet in metapelites from the Gongshan block is euhedral to subhedral with variable grain size from 0.5 to 2 mm. Six porphyroblastic garnets from six samples were chosen for zoning profile analyses (Appendix A, Tables A2–A7). As shown in Fig. 7a and b,

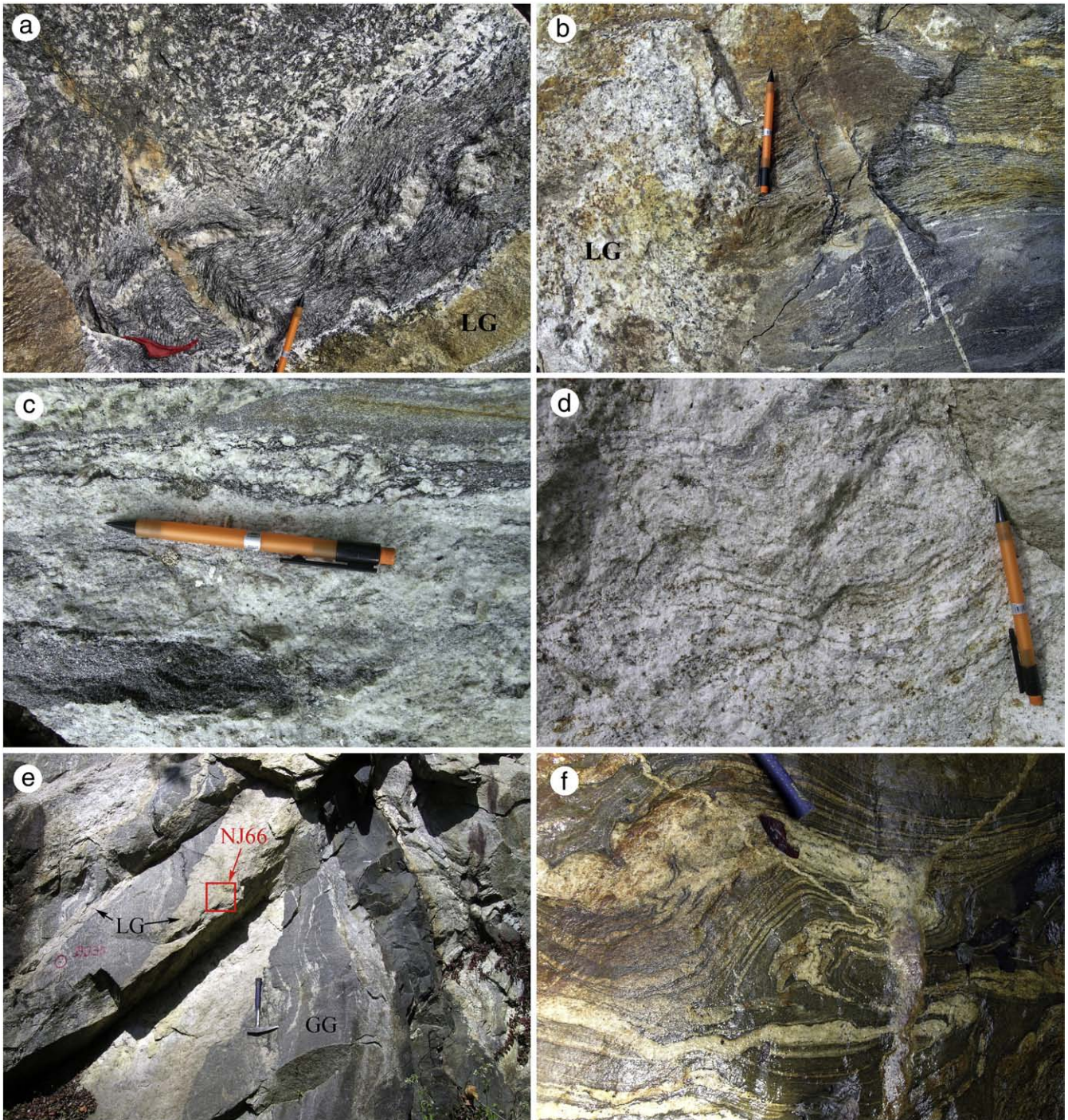


**Fig. 6.** Photographs showing anatisis of metapelite from the Gaoligong Group. (a) Melt pockets within the high-grade garnet-bearing metapelite. (b) Field relationship between garnet-muscovite leucogranite and pelitic gneiss. (c) Garnet leucogranite bands with metapelite. (d) Residual foliations in the leucosome with the mineral assemblage of  $gt + sill + bi + per + pl + mu + q$ . (e) The 22.7-Ma garnet leucogranite veins cutting the 490-Ma granitic gneiss and the regional foliation. (f) Two generations of leucosome veins in the Carboniferous metasandstone.

garnet from the staurolite-bearing schist (ST56 and NJ49) exhibits pronounced bell-shaped profiles with antithetic zoning of spessartine relative to almandine and pyrope contents; the  $X_{sps}$  decreases from the core (0.198–0.235) to the rim (0.084–0.118), whereas the  $X_{alm}$  and the  $X_{pyr}$  increase from the core (Alm 0.651–0.704, Pyr 0.044–0.081) to rim (Alm 0.783, Pyr 0.098–0.103).  $X_{gro}$  in garnet from ST56 decreases from 0.075 in the core to 0.042 at the rim and  $X_{gro}$  from NJ49 increases from 0.016 to 0.028 but decreases to 0.005 at the outer rim. Garnet from the K-feldspar-bearing schist/gneiss (NJ39, NJ43 and

NJ54) and leucogranite (NJ44) shows relative flat profiles with weak variations (Fig. 7c–e). In the sample NJ43 (Fig. 7c), garnet is zoned with  $X_{alm}$  increasing from 0.791 in the core to 0.825 at the rim,  $X_{pyr}$  decreasing from 0.132 to 0.106,  $X_{sps}$  from 0.063 to 0.046 and  $X_{gro}$  from 0.027 to 0.017. Garnet from sample NJ54, just opposite to others, is zoned with  $X_{sps}$  increasing from 0.084 in the core to 0.112 at the rim,  $X_{alm}$  decreasing from 0.765 to 0.746 and  $X_{pyr}$  from 0.136 to 0.113 (Fig. 7e). Garnet from NJ39 shows flat profiles from the core ( $X_{alm}$  0.687,  $X_{pyr}$  0.181,  $X_{sps}$  0.078,  $X_{gro}$  0.036) to the rim ( $X_{alm}$  0.709,  $X_{pyr}$

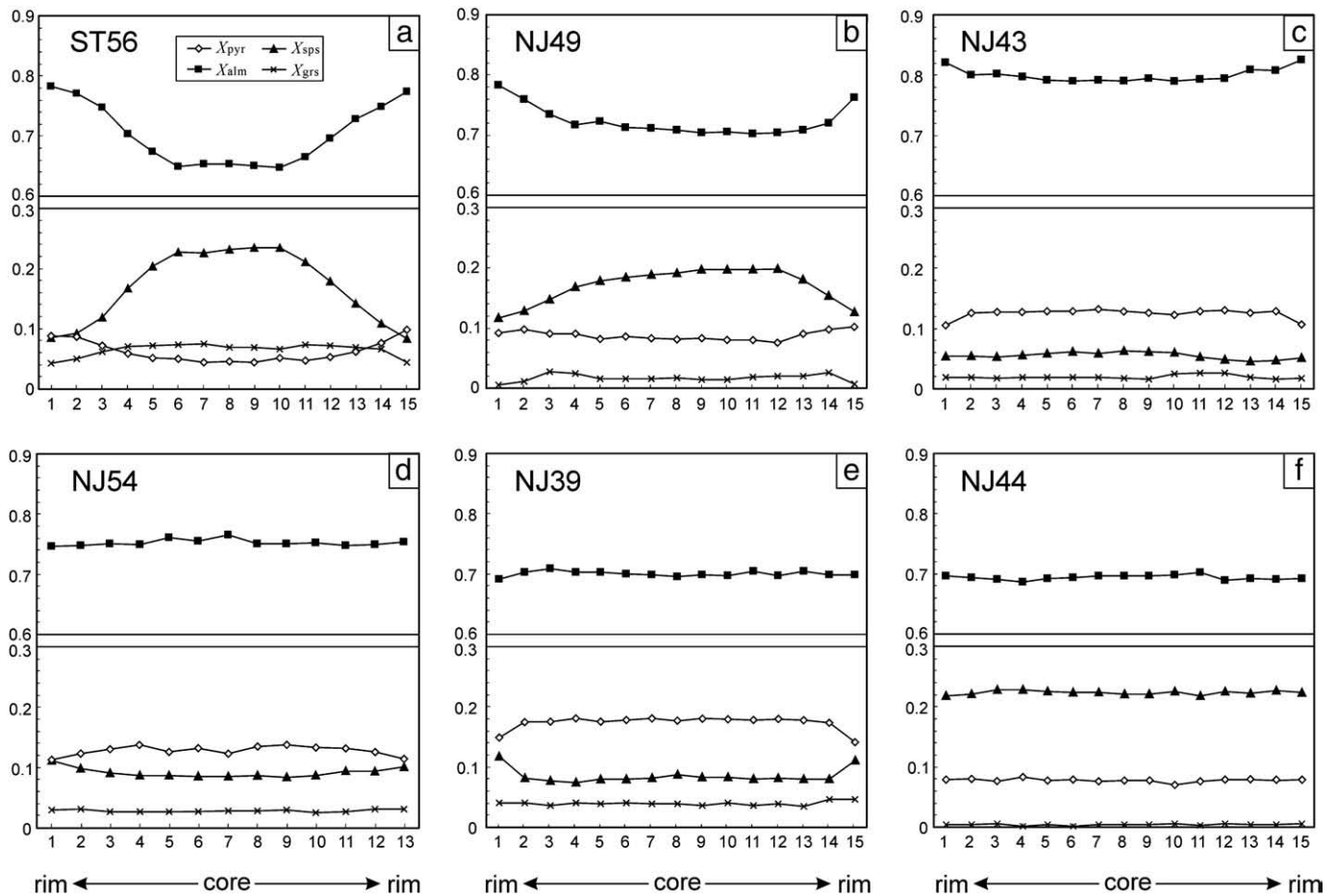


Fig. 7. Garnet compositional profiles in terms of  $X_{alm} = Fe^{2+} / (Fe^{2+} + Mn + Mg + Ca)$ ,  $X_{sps} = Mn / (Fe^{2+} + Mn + Mg + Ca)$ ,  $X_{grs} = Ca / (Fe^{2+} + Mn + Mg + Ca)$  and  $X_{pyr} = Mg / (Fe^{2+} + Mn + Mg + Ca)$ . Garnet grains are from staurolite-bearing schist (ST56 and NJ49), K-feldspar-bearing schist/gneiss (NJ39, NJ43, NJ54) and the leucogranite (NJ44).

0.174,  $X_{sps}$  0.083,  $X_{gro}$  0.046); spessartine increases and pyrope decreases rapidly at the outermost rim (Fig. 7e). Garnet from leucogranite (NJ44) also shows flat compositional profiles with relatively high spessartine and low grossular ( $X_{alm}$  0.228–0.218,  $X_{pyr}$  0.181–0.174,  $X_{sps}$  0.078–0.083,  $X_{gro}$  0.036–0.046) (Fig. 7f).

## 5.2. Other minerals

Composition of other minerals in the metapelites is weak zoned or unzoned from the core to the rim. Biotite occurs mainly in the matrix; no grain was found as inclusion in garnet. Biotite compositions from all analyzed samples have variable  $TiO_2$  (1.17–3.04 wt%), FeO (17.12–23.22 wt%) and  $Fe/[Fe + Mg]$  (0.50–0.70) and  $TiO_2$  content shows a rough increase with the metamorphic grade from the north to south. White mica from the pelitic schist or gneiss is muscovite with Si content ranging from 3.05 to 3.14 cations per formula unit (p.f.u.) on the basis of 11 oxygen. Muscovite that occurs as second generation along the shearing foliation is enriched in  $Na_2O$  (e.g.,  $Na/[Na + K] = 0.24–0.26$  in sample NJ49) than that in other samples. Plagioclase is unzoned but shows large compositional variation (e.g.,  $Ab_{47–83}$ ,  $An_{16–52}$  and  $Or_{0.3–2.6}$ ) in different samples. Albite of second generation is Na rich ( $Ab > 90$ ) and is associated with muscovite and chlorite along shearing foliations (e.g., in sample NJ49). K-feldspar has typical compositions ( $Or_{87.7–92.3}$ ,  $Ab_{7.7–12.2}$  and  $An_{<0.1}$ ). Perthite was found in the metapelite NJ43 and the leucogranite NJ44, which comprises almost pure albite exsolutions ( $Or_{0–2.2}Ab_{97–98}An_{0–2.5}$ ) in a K-feldspar-rich host. Stau-

rolite has high Fe (e.g.,  $Mg^{\#} = Mg/[Mg + Fe] = 0.14–0.16$  in sample ST56 and NJ49).

## 5.3. Pressure (P) and temperature (T) estimates

Metamorphic conditions of all garnet-bearing metapelite samples (see Table 1 and Fig. 5) were determined by average  $P-T$  methods using mineral compositional data and the THERMOCALC (version 3.23; Powell et al., 1998) with the internally consistent thermodynamic dataset (Holland and Powell, 1998; November 2003 updated file tcds55.txt). Quartz and the fluid phase that is assumed to be pure  $H_2O$ , are considered to be in excess. In finding an average  $P-T$  of a mineral assemblage, an independent set of reactions between mineral end-members in the assemblage are used. The appropriate linear sets of independent reactions used are given in Appendix B. All mineral formulae in Table A1 and end-member activities were calculated using AX by Holland (see <http://www.esc.cam.ac.uk/astaff/holland/ax.html>). Rim or near rim compositions of the garnet, staurolite, mica and plagioclase are used in average  $P-T$  calculations. Gt-bi geothermometry of Holdaway (2000) was also used for temperature calculations.

Mineral assemblages and calculated average  $P-T$  conditions are given in Table 1 and Fig. 8.  $P-T$  estimates for the staurolite bearing schists (ST56 and NJ49) give  $P = 7.1–8.3$  kbar and  $T = 650–660$  °C. Other samples with K-feldspar +  $Al_2SiO_5$  assemblage yield  $T = 685–750$  °C and  $P = 6.5–8.4$  kbar. The  $P-T$  diagram exhibits a tendency of

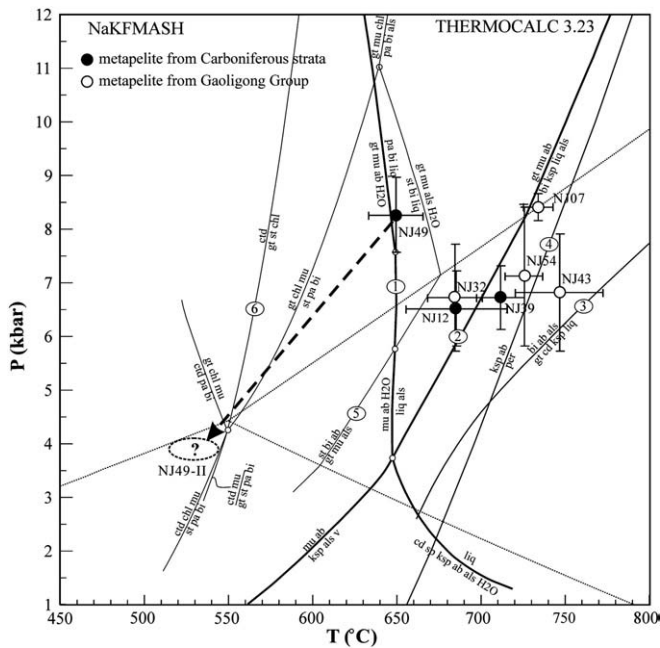


**Fig. 8.** *P*–*T* diagram of metapelites from Carboniferous strata and Gaoligong Group. Reactions are calculated using THERMOCALC 3.23 of Powell et al. (1998) for the NaKFMASH system. Four samples record the conditions of anatexis by muscovite dehydration reaction (2)  $\mu + gt + ab = bi + ksp + als + liq$ . Sample NJ49 shows a two-stage metamorphism: the second generation of  $\mu + ab + q (+chl)$  (NJ49-II, Fig. 3a, b) overprints the peak assemblage at low *P*–*T* conditions during the subsequent lateral shear deformation. See Table 1 for mineral abbreviations except for als, which stands for  $Al_2SiO_5$ .

increasing temperature from north to south, as expected from field observations.

## 6. Geochronology

### 6.1. Analytical methods

Zircon crystals were extracted from crushed samples by using combined methods of magnetic and heavy liquid separation before finally hand-picked under a binocular. These zircons were then embedded in 25 mm epoxy discs and polished down to approximately half thickness for CL and SHRIMP studies. The internal zoning was examined using a CL spectrometer (Garton Mono CL3+) equipped on a Quanta 200F ESEM with 2-min scanning time at conditions of 15 kV and 120 nA at Peking University (Figs. 9 and 10).

Zircons from most samples were analyzed for U, Pb and Th isotopes using SHRIMP II at Beijing SHRIMP Centre, Chinese Academy of Geosciences. Instrumental conditions and measurement procedures follow Compston et al. (1992). The spot size of the ion beam was about 25  $\mu\text{m}$  in diameter, and the data were collected in sets of five scans through the masses with 2 nA primary  $O_2^-$  beams. The reference zircon was analyzed first and again after every three unknowns. The measured  $^{206}\text{Pb}/^{238}\text{U}$  ratios in the samples were corrected using reference zircon standard SL13 from a pegmatite from Sri Lanka ( $^{206}\text{Pb}/^{238}\text{U} = 0.0928$ ; 572 Ma) and zircon standard TEMORA (417 Ma) from Australia (Black et al., 2003). The common-Pb correction used the  $^{206}\text{Pb}/^{204}\text{Pb}$  ratio and assumed a two-stage evolution model (Stacey and Kramers, 1975). For the zircon rims of samples NJ54, because the uncertainty in measuring the small amount of  $^{204}\text{Pb}$  is too large,  $^{208}\text{Pb}$  common lead correction has been used for the Concordia plot, based on the fact that all measured  $^{208}\text{Pb}/^{206}\text{Pb}$  versus Th/U were perfectly correlated (Compston et al., 1992; Rubatto et al., 1999).

Laser ablation (LA)-ICP-MS zircon U-Pb geochronology from one meta-pelitic sample (NJ56) and one tourmaline granite sample (NJ74)

was carried out at the Geologic Lab Center, China University of Geosciences (Beijing). The instrument couples a quadrupole ICP-MS (Agilent 7500a) and a UP-193 Solid-State laser (193 nm, New Wave Research Inc.) with the automatic positioning system. For the present work, laser spot size was set to  $\sim 36 \mu\text{m}$  for most analyses and to 25  $\mu\text{m}$  for metamorphic rims, laser energy density at 8.5 J/cm<sup>2</sup> and repetition rate at 10 Hz. The procedure of laser sampling is 5-s pre-ablation, 20-s sample-chamber flushing and 40-s sampling ablation. The ablated material is carried into the ICP-MS by the high-purity Helium gas stream with flux of 0.8 L/min. The whole laser path was fluxed with  $N_2$  (15 L/min) and Ar (1.15 L/min) in order to increase energy stability. The counting time for U, Th,  $^{204}\text{Pb}$ ,  $^{206}\text{Pb}$ ,  $^{207}\text{Pb}$  and  $^{208}\text{Pb}$  is 20 ms, and is 15 ms for other elements. Calibrations for the zircon analyses were carried out using NIST 610 glass as an external standard and Si as internal standard. U-Pb isotope fractionation effects were corrected using zircon 91500 (Wiedenbeck et al., 1995) as external standard. Zircon standard TEMORA (417 Ma) from Australia (Black et al., 2003) is also used as a secondary standard to supervise the deviation of age measurement/calculation. Ten analyses for the standard TEMORA yielded apparent  $^{206}\text{Pb}/^{238}\text{U}$  ages of 408–420 Ma with a weighted mean of  $415.7 \pm 4.2$  Ma (MSWD = 0.36). Isotopic ratios and element concentrations of zircons were calculated using GLITTER (ver. 4.4, Macquarie University). Concordia ages and diagrams were obtained using Isoplot/Ex (3.0) (Ludwig, 2003). The common lead was corrected using LA-ICP-MS Common Lead Correction (ver. 3.15), followed the method of Andersen (2002).

The analytical data are given in Tables 2, 3, 4 and 5, and presented on U-Pb Concordia diagrams with  $1\sigma$  errors in Figs. 10 and 11. The mean ages are weighted means at 95% confidence levels (Ludwig, 2003).

### 6.2. Granulite-facies Pelitic Gneisses of the Gaoligong Group

Zircons from the garnet-sillimanite gneisses (samples NJ32, NJ54 and NJ56) are subhedral to oval with long axes varying from 50  $\mu\text{m}$  up to 250  $\mu\text{m}$  and length/width ratio from 1.5 to 2.5. CL images of zircons from these pelitic gneisses show clear internal zoning with inherited detrital cores and metamorphic rims (Fig. 9). The irregularly-shaped detrital cores display luminescence of varying strength and clear oscillatory bands or sectors. The metamorphic rims are generally characterized by irregular and weak zoning. Mineral inclusions of garnet, sillimanite, quartz and K-feldspar were detected in rim portions by a micro-Raman spectroscopy (Ranisow RM-1000) with the 514.5 nm line of an Ar-ion laser at Peking University (Fig. 9b).

Zircons from two pelitic gneisses (NJ32 and NJ54) were analyzed using the SHRIMP method. The cores show huge U variation (93 to 2037 ppm; Th/U ratio from 0.19 to 1.49). Twenty-two core analyses yield ages varying from  $74 \pm 1.2$  Ma ( $^{206}\text{Pb}/^{238}\text{U}$ ) to  $2752 \pm 21$  Ma ( $^{207}\text{Pb}/^{206}\text{Pb}$ ). In U-Pb concordia diagrams, analyses of four zircon cores define a concordia line with an upper-intercept age of  $2690 \pm 35$  Ma and a lower-intercept age of  $1152 \pm 120$  Ma (MSWD = 0.49). Analyses of two zircon cores define a concordia curve with an upper-intercept age of  $1873 \pm 19$  Ma and a lower-intercept age of  $467 \pm 50$  Ma (MSWD = 0.09) (Fig. 10a). Other concordant spot ages include  $1557 \pm 21$  Ma,  $1053 \pm 18$  Ma,  $636 \pm 10$ – $691 \pm 11$  Ma,  $470 \pm 11$  Ma,  $203 \pm 5$ – $255 \pm 7$  Ma and  $74 \pm 1$ – $140 \pm 4$  Ma.

By contrast, zircon rims of sample NJ54 have relatively uniform U (730–1063 ppm) and low Th (3–9 ppm), thus giving significantly lower Th/U ratios (0.004–0.012) than cores, which have been commonly interpreted as typical features of “metamorphic overgrowth” in granulite-facies (Williams and Claesson, 1987; Vavra et al., 1996; Williams, 1996) and eclogite-facies rocks (Rubatto et al., 1999; Song et al., 2006). Eleven rim analyses give  $^{206}\text{Pb}/^{238}\text{U}$  ages of 20.4 to 23.8 Ma with a weighted mean of  $22.5 \pm 0.6$  Ma (MSWD = 1.9) (Table 2, Fig. 10b), close to the Oligocene–Miocene boundary. Zircon rims of NJ32 were too narrow to analyze.

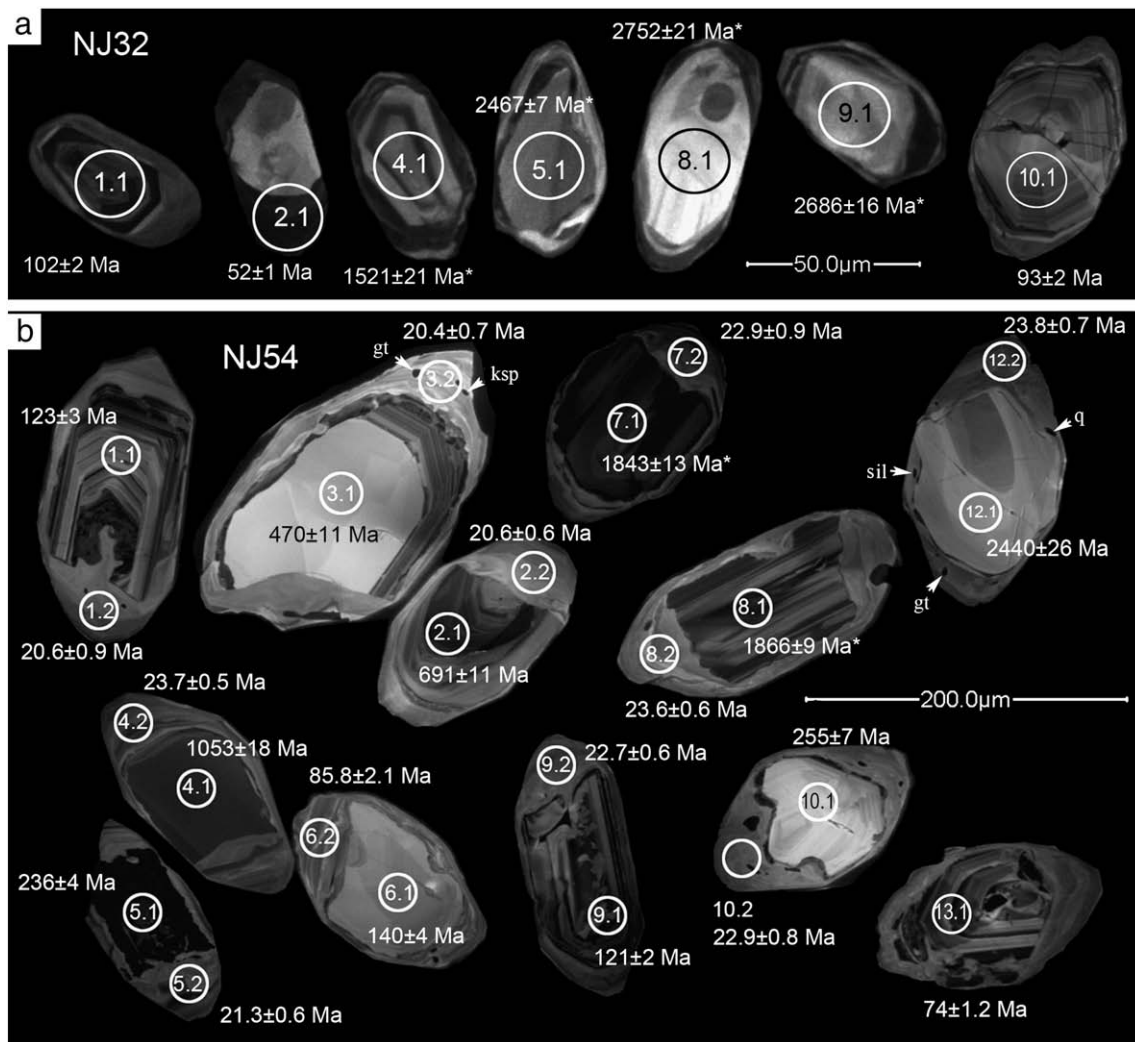


**Fig. 9.** Representative CL images for zircons from pelitic gneisses NJ32 (a) and NJ54 (b) of the Gaoligong Group. Mineral inclusions of garnet (gt), K-feldspar (ksp), sillimanite (sil) and quartz (q) occur in the rim domains of zircon crystals.

Zircons from a similar metapelite sample NJ56 were analyzed by LA-ICP-MS (Table 3). The cores also give huge variations in U (37 to 2064 ppm) and Th/U (0.10–2.50). Sixty core analyses yield  $^{206}\text{Pb}/^{238}\text{U}$  ages varying from 64 Ma to 2563 Ma. In contrast to SHRIMP dating of NJ32 and NJ54, eight detrital magmatic zircons from sample NJ56 gives Jurassic ages (157 to 165 Ma). It should be noted that all these zircon cores with Jurassic and Cretaceous ages (165–64 Ma) show clear magmatic oscillatory bands, high Th/U ratios (0.35–2.50) and are large enough for precise dating. Six zircon rims from sample NJ56 show relatively uniform U (663–919 ppm) and significantly lower Th/U ratios (0.004–0.009) than the inherited cores and yield  $^{206}\text{Pb}/^{238}\text{U}$  ages of 20.7 to 22.3 Ma with a weighted mean of  $21.6 \pm 0.6$  Ma (MSWD = 1.8).

### 6.3. Leucogranite within the Gongshan block

Zircons from leucogranite sample NJ66 are euhedral, but have complex internal structures; all have a dirty “corroded” core and a dark luminescent rim with magmatic oscillatory bands (Fig. 12a). SHRIMP analysis gives relatively uniform but very high U (3169 to 5015 ppm) and low Th/U (0.007–0.024). Two analyses on the core domains yield  $^{206}\text{Pb}/^{238}\text{U}$  ages of  $44.8 \pm 0.7$  Ma and  $53.2 \pm 0.9$  Ma. Analysis of seven rims gives ages varying from 22.0 to 34.6 Ma, five of which give a weighted mean of  $22.7 \pm 0.8$  Ma (MSWD = 1.6, Fig. 11a). These data may suggest a two-stage growth of zircons in

the leucogranite at ~45–53 Ma and the peak anatectic age of 22.7 Ma. However, it is possible that the cores could have been crystallized from earlier melt of the same magmatism, but the later melt may be compositionally different and may thus have corroded the growing zircons with Pb leaching. As a result, the cores give older and inconsistent (~8 Myrs difference) apparent ages of 45 and 53 Ma. In any case, further work is needed to verify this hypothesis, but the ~22.7 Ma rim age is a genuine age of the leucogranite petrogenesis.

### 6.4. Tourmaline granite within high-grade metamorphic rocks

Zircon crystals from the tourmaline granite (ST122) are euhedral and about 100–250 μm in length and 60–120 μm in width. They display oscillatory bands in CL images (Fig. 12b) and contain extremely high U (1827–21523 ppm) and Th (233–2666 ppm) with Th/U ranging from 0.05 to 0.25 by SHRIMP analyses. These data are consistent with the magma parental to the granite being highly evolved and enriched in volatiles (e.g., tourmaline bearing) and incompatible elements (e.g., high Th and U). Twelve analyses of zircon crystals yield  $^{206}\text{Pb}/^{238}\text{U}$  ages of 22.8 to 26.9 Ma and ten spots give a weighted mean of  $24.4 \pm 0.7$  Ma (MSWD = 1.7) (two old spots were discarded because they are possibly influenced by the old core) (Table 4, Fig. 11b). LA-ICP-MS analysis of zircons from another tourmaline granite sample NJ74 gives high U (728–11116 ppm) and

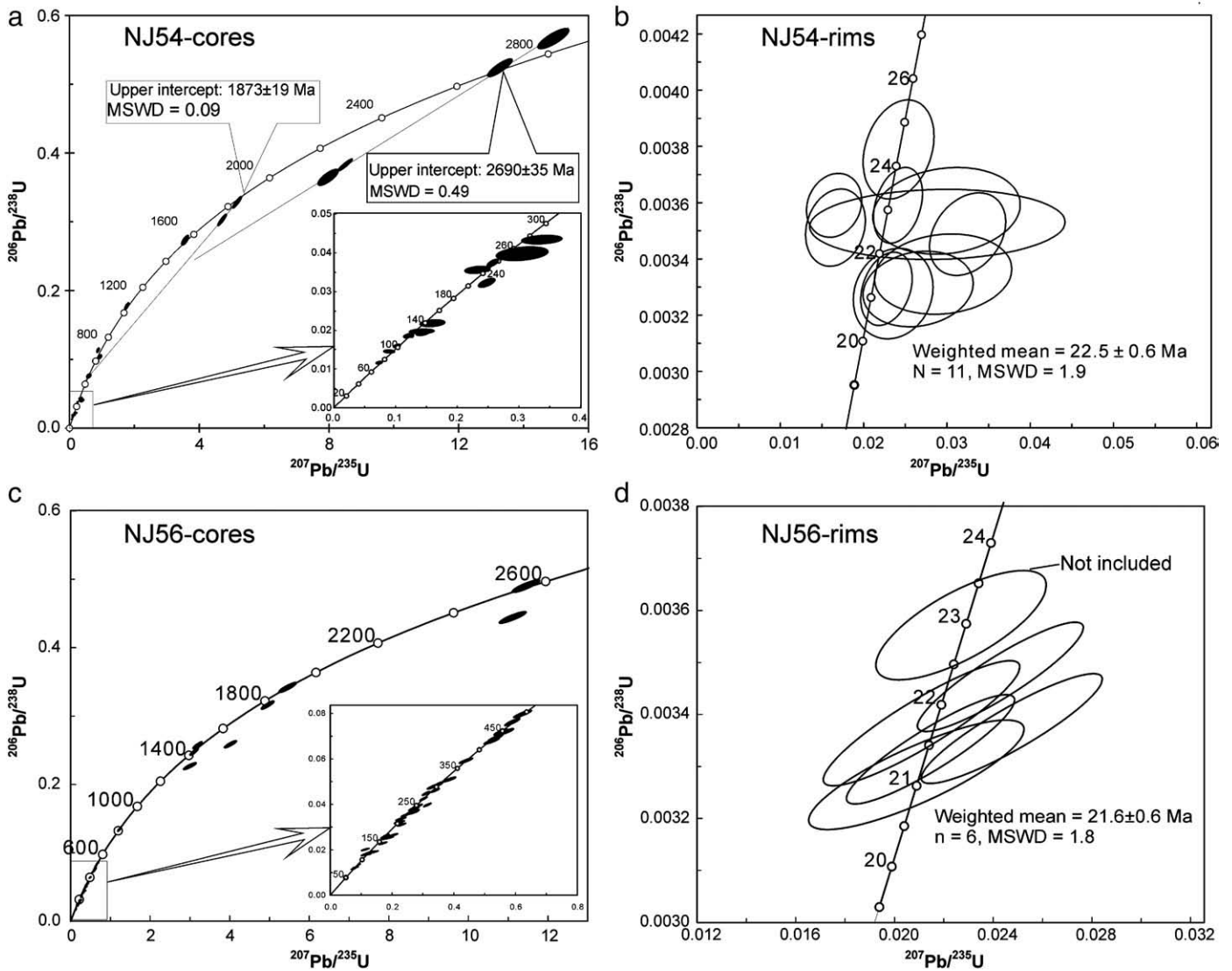


**Fig. 10.** (a) Concordia diagram for cores of detrital zircons from the pelitic gneisses (NJ32 and NJ54) of the Gaoligong Group by SHRIMP dating. All the young ages are concordant in the inset. (b) Concordia diagram for metamorphic rims of zircons from the pelitic gneiss NJ54 by IA-ICP-MS. (c) Concordia diagram for cores of detrital zircons from the pelitic gneisses (NJ56) by IA-ICP-MS dating. The young ages are concordant in the inset. (d) Concordia diagram for metamorphic rims of zircons from the pelitic gneiss NJ56 by IA-ICP-MS.

Th/U (0.04–0.52) (Table 5). Five analyses give  $^{206}\text{Pb}/^{238}\text{U}$  ages of 34.3–41.8 Ma and twelve analyses give ages of 24.2–27.2 Ma with a weighted mean of  $25.5 \pm 0.5$  Ma (MSWD = 1.5), suggesting two stages of zircon growth from the anatexic melts (Fig. 11c). One bright-luminescent core contains low Th and U and yields a  $^{207}\text{Pb}/^{206}\text{Pb}$  apparent age of  $2455 \pm 34$  Ma.

## 7. Discussion

### 7.1. Neoproterozoic basement in the NIC?

Precambrian basement of the Indochina continent was thought to be mainly formed in the early Proterozoic; Sm-Nd TDM model ages of high-grade metamorphic rocks in this region range from 2.3 to 1.0 Ga (Zhai et al., 1990; Zhang and Schärer, 1999), and detrital zircon and baddeleyite grains from sediments from four major rivers in the Indochina continent yield ages younger than 2.5 Ga (Bodet and Schärer, 2000). Although Lan et al. (2001) reported Neoproterozoic ages from gneisses in northern Vietnam, they inferred that this Neoproterozoic complex was genetically associated with the Late Archean Kangding complex at the western margin of the Yangtze Craton and therefore concluded that the Indochina continent was sinistrally offset ~600 km

by the Red River shear zone. However, geochronological data indicated that the Kangding complex in western Sichuan actually formed in the Neoproterozoic (Li et al., 2003; Chen et al., 2005; Zhao et al., 2006) rather than in the Late Archean.

Concordant  $^{207}\text{Pb}/^{206}\text{Pb}$  ages of 2752–2686 Ma and the upper-intercept age of  $2690 \pm 35$  Ma from detrital cores of samples NJ32 and NJ54, together with high Th/U ratios (0.63–1.35) and magmatic CL internal structures of these four old detrital zircon cores, indicate a Neoproterozoic magmatic event. The concordant  $^{207}\text{Pb}/^{206}\text{Pb}$  ages of 1866–1896 Ma and a similar upper-intercept age of  $1873 \pm 19$  Ma suggest another magmatic event in the Paleoproterozoic. These new findings indicate the presence of early Precambrian basement in the NIC region.

### 7.2. Crustal evolution and provenance of the NIC

The concordant ages of detrital zircon cores from pelitic gneisses of the Gaoligong Group (NJ32, NJ54 and NJ56) and from the gneissic granite (NJ65) record multiple episodes of magmatism from the Neoproterozoic to the Mesozoic in the source region.

Neoproterozoic detrital zircon ages of  $1053 \pm 18$  Ma,  $789 \pm 10$  Ma and  $690$ – $635$  Ma, together with the core ages of  $774$ – $796$  Ma from the

**Table 2**  
U-Th-Pb SHRIMP zircon data of the pelitic gneisses (NJ32 and NJ54) from the Gaoligong Group.

Spot		U ppm	Th ppm	Th/U	<sup>206</sup> Pb* ppm	Comm. <sup>206</sup> Pb (%)	<sup>207</sup> Pb*/ <sup>235</sup> U	<sup>206</sup> Pb*/ <sup>238</sup> U	<sup>207</sup> Pb*/ <sup>206</sup> Pb*	<sup>206</sup> Pb/ <sup>238</sup> U age (Ma)	<sup>207</sup> Pb/ <sup>206</sup> Pb age (Ma)
NJ32-1.1	D	777	866	1.15	10.7	1.19	0.10 ± 0.003	0.0159 ± 0.0003	0.0464 ± 0.0013	102 ± 2	
NJ32-2.1	M	679	86	0.13	4.9	5.16	0.04 ± 0.005	0.0081 ± 0.0001	0.0397 ± 0.0044	52 ± 1	
NJ32-3.1	D	331	198	0.62	29.7	2.40	0.94 ± 0.025	0.1036 ± 0.0016	0.0659 ± 0.0014	636 ± 10	
NJ32-4.1	D	426	276	0.67	100.1	0.83	3.56 ± 0.067	0.2731 ± 0.0042	0.0946 ± 0.0010	1557 ± 21	1521 ± 21
NJ32-5.1	D	495	98	0.20	162.8	0.55	8.50 ± 0.134	0.3828 ± 0.0058	0.1611 ± 0.0007	2089 ± 27	2467 ± 7
NJ32-7.1	D	279	297	1.10	4.8	1.34	0.09 ± 0.022	0.0192 ± 0.0004	0.0341 ± 0.0084	123 ± 3	
NJ32-8.1	D	98	129	1.35	48.0	3.32	14.92 ± 0.311	0.5661 ± 0.0094	0.1911 ± 0.0024	2892 ± 39	2752 ± 21
NJ32-9.1	D	215	132	0.63	97.1	1.49	13.27 ± 0.247	0.5242 ± 0.0083	0.1836 ± 0.0018	2717 ± 35	2686 ± 16
NJ32-10.1	D	1129	319	0.29	15.0	0.92	0.09 ± 0.008	0.0145 ± 0.0001	0.0125 ± 0.0065	93 ± 2	
NJ32-11.1	D	190	128	0.69	5.9	1.15	0.17 ± 0.074	0.0350 ± 0.0009	0.0345 ± 0.0152	222 ± 5	
NJ54-1.1	D	454	431	0.98	7.6	0.34	0.13 ± 0.010	0.0192 ± 0.0004	0.0483 ± 0.0037	123 ± 3	
NJ54-2.1	D	1617	372	0.24	157.5	0.11	0.88 ± 0.017	0.1132 ± 0.0019	0.0564 ± 0.0006	691 ± 11	
NJ54-3.1	D	156	129	0.85	10.2	0.12	0.59 ± 0.035	0.0757 ± 0.0019	0.0568 ± 0.0030	470 ± 11	
NJ54-4.1	D	803	1360	1.75	122.4	-0.34	1.84 ± 0.038	0.1780 ± 0.0033	0.0722 ± 0.0007	1053 ± 18	
NJ54-5.1	D	2037	284	0.14	65.5	0.34	0.25 ± 0.007	0.0373 ± 0.0006	0.0495 ± 0.0012	236 ± 4	
NJ54-6.1	D	221	100	0.46	4.3	3.81	0.18 ± 0.030	0.0220 ± 0.0006	0.0593 ± 0.0099	140 ± 4	
NJ54-7.1	D	679	136	0.21	176.9	0.11	4.71 ± 0.087	0.3028 ± 0.0052	0.1127 ± 0.0008	1705 ± 26	1843 ± 13
NJ54-8.1	D	1193	1066	0.92	336.8	-0.11	5.17 ± 0.089	0.3284 ± 0.0054	0.1141 ± 0.0006	1831 ± 26	1866 ± 9
NJ54-9.1	D	1035	734	0.73	16.8	1.93	0.15 ± 0.005	0.0189 ± 0.0003	0.0593 ± 0.0016	121 ± 2	
NJ54-10.1	D	93	135	1.49	3.3	3.48	0.38 ± 0.031	0.0403 ± 0.0011	0.0688 ± 0.0052	255 ± 7	
NJ54-11.1	D	2483	1689	0.70	68.5	-0.33	0.23 ± 0.009	0.0321 ± 0.0008	0.0522 ± 0.0015	203 ± 5	
NJ54-12.1	D	101	48	0.49	31.6	0.78	7.97 ± 0.203	0.3647 ± 0.0074	0.1585 ± 0.0024	2005 ± 35	2440 ± 26
NJ54-13.1	D	3385	1825	0.56	34.0	1.02	0.07 ± 0.003	0.0116 ± 0.0002	0.0456 ± 0.0016	74 ± 1.2	
NJ54-1.2	R	777	9	0.012	2.3	3.16	0.030 ± 0.005	0.0034 ± 0.0001		21.5 ± 0.6	
NJ54-2.2	R	854	3	0.004	2.4	3.80	0.027 ± 0.004	0.0033 ± 0.0001		21.6 ± 0.6	
NJ54-3.2	R	913	5	0.006	2.6	3.01	0.024 ± 0.003	0.0033 ± 0.0001		21.4 ± 0.7	
NJ54-4.2	R	1063	5	0.005	3.4	4.20	0.017 ± 0.002	0.0036 ± 0.0001	0.0332 ± 0.0044	23.1 ± 0.5	
NJ54-5.2	R	921	4	0.004	2.6	1.57	0.023 ± 0.002	0.0033 ± 0.0001	0.0501 ± 0.0043	21.2 ± 0.6	
NJ54-6.2	M	1024	7	0.007	3.2	1.12	0.075 ± 0.006	0.0124 ± 0.0003	0.0438 ± 0.0033	79.7 ± 2.3	
NJ54-7.2	R	864	29	0.035	10.0	7.60	0.024 ± 0.002	0.0036 ± 0.0001	0.0487 ± 0.0037	23.1 ± 0.6	
NJ54-8.2	R	760	4	0.005	2.9	2.92	0.033 ± 0.003	0.0035 ± 0.0001	0.0542 ± 0.0048	22.9 ± 0.9	
NJ54-9.2	R	950	5	0.005	2.9	2.60	0.017 ± 0.002	0.0035 ± 0.0001	0.0343 ± 0.0048	22.6 ± 0.6	
NJ54-10.2	R	927	8	0.008	4.5	6.44	0.029 ± 0.010	0.0035 ± 0.0001	0.0262 ± 0.0092	22.8 ± 0.8	
NJ54-11.2	R	745	3	0.005	2.4	3.99	0.030 ± 0.006	0.0036 ± 0.0001	0.0608 ± 0.0117	23.0 ± 0.7	
NJ54-12.2	R	730	4	0.005	2.4	1.28	0.024 ± 0.003	0.0038 ± 0.0001	0.0463 ± 0.0052	24.4 ± 0.8	

All errors are 1 sigma of standard deviation. D = detrital core, R = rim, M = mixing analysis of core and rim.  
Pb\* is the radiogenic lead.

gneissic granite (Song et al., 2007) indicate geologic events that are in fact widespread throughout the ancient Gondwana continent (Li et al., 1999; Avigad et al., 2003; Hanson et al., 2004). The 487 ± 11 Ma peraluminous (S-type) granite in the Gongshan block is interpreted as resulting from a crustal melting event (Song et al., 2007). Similar granites are also reported in the Baoshan block with zircon U-Pb ages of 470–490 Ma (Chen et al., 2004), which indicates that the Gongshan and Baoshan blocks have experienced the same magmatic event at this time. These granites correspond to the widespread subduction-related magmatism on the northern margin of Gondwana (Schelling, 1992; Hoffman et al., 1998; DeCelles et al., 2000) in the early Paleozoic.

The detrital zircon ages of 300–195 Ma from the pelitic gneisses (samples NJ32, NJ54 and NJ56) and 259–200 Ma ages of granites within the Gaoshan and Baoshan blocks (YBGMR, 1990; Peng et al., 2006) suggest an important magmatic event that may have occurred in the Triassic (~250–200 Ma). Triassic granites have also been recognized in the southeastern Indochina continent, and have been interpreted as the result of collision between the Indochina continent and the South China Craton (Lan et al., 2000; Carter et al., 2001). The twenty-eight 165–64-Ma detrital zircon cores from the three pelitic gneiss samples are consistent with the Gaoligongshan being magmatically active during the Late Jurassic to Cretaceous (140–65 Ma) (Yan et al., 2002; Chen et al., 2006). This magmatic belt is temporally comparable to the magmatic belt of the Gangdese granitoids in the Lhasa Block in southern Tibet (see below).

The age spectrum of a continental block records its thermo-tectonic histories and thus can be used to trace its origin and tectonic affiliation in the context of plate tectonic reconstructions. The

Neoproterozoic to Early Paleozoic ages (2690–430 Ma) of both detrital zircons from the Gaoligong pelitic gneisses and zircons from the gneissic granite resemble those of the Himalayan Orogen in Nepal, which was suggested to have been accreted onto northern Gondwana and intruded by crustal melts during the Cambrian-Ordovician time (DeCelles et al., 2000). This age spectrum differs from those of the Yangtze Craton where there is no evidence for early Paleozoic magmatism (Chen and Jahn, 1998; Li et al., 1999). However, data from DeCelles et al. (2000) and Yin (2006) indicate that the Himalayan orogenic belt and the northern Indian Plate lack records of the Late Paleozoic to Mesozoic (~300–65 Ma) magmatism (Fig. 13) although some mafic volcanic and intrusive rocks of early Cretaceous ages (130–145 Ma) have been reported (Zhu et al., 2008); this suggests that the NIC should have separated from Gondwana continent and collided with Eurasian Plate at the Triassic time. On the other hand, the Lhasa Block, in comparison with the NIC blocks, has similar ages of magmatism especially from Neoproterozoic to Mesozoic times (850–70 Ma) (Xu et al., 1985; Yin and Harrison, 2000; Hu et al., 2004; Kapp et al., 2005a,b; Chu et al., 2006; Guynn et al., 2006) (Fig. 13) despite the recent recognition of the presence of the pre-Proterozoic basement in the Lhasa block (Yang and Li, 2006; Duo et al., 2007; Zhu et al., 2009). Therefore, it is possible that the NIC and Lhasa Block in southern Tibet may have been an integral part of the same tectonic block that had disintegrated from Gondwana and amalgamated with Eurasia in the Triassic. If our interpretation is proved to be correct, it offers a new perspective on the origin and tectonic history of the Lhasa Block in response to the India-Asia continental collision and continued convergence.

**Table 3**  
U-Th-Pb LA-ICP-MS zircon data of the pelitic gneiss NJ56 from the Gaoligong Group.

Analysis	Th ppm	U ppm	Th/U	$^{207}\text{Pb}/^{206}\text{Pb}$	$^{207}\text{Pb}/^{235}\text{U}$	$^{206}\text{Pb}/^{238}\text{U}$	$^{207}\text{Pb}/^{206}\text{Pb}$ age (Ma)	$^{206}\text{Pb}/^{238}\text{U}$ age (Ma)
<i>Metamorphic rims</i>								
NJ56-01A	3.6	876	0.004	0.0466 ± 0.0050	0.0214 ± 0.0023	0.00333 ± 0.00007		21.4 ± 0.4
NJ56-02A	5.8	663	0.009	0.0461 ± 0.0048	0.0227 ± 0.0023	0.00357 ± 0.00007		23.0 ± 0.4
NJ56-12A	6.0	919	0.007	0.0524 ± 0.0075	0.0208 ± 0.0029	0.00332 ± 0.00007		21.3 ± 0.5
NJ56-13A	4.3	610	0.007	0.0451 ± 0.0058	0.0211 ± 0.0027	0.00338 ± 0.00008		21.8 ± 0.5
NJ56-17A	6.3	771	0.008	0.0506 ± 0.0047	0.0243 ± 0.0022	0.00347 ± 0.00007		22.3 ± 0.4
NJ56-18A	6.8	740	0.009	0.0532 ± 0.0053	0.0247 ± 0.0024	0.00337 ± 0.00007		21.7 ± 0.4
NJ56-20A	4.9	835	0.006	0.0532 ± 0.0053	0.0247 ± 0.0024	0.00321 ± 0.00007		20.7 ± 0.4
<i>Detrital cores</i>								
NJ56-01B	27.4	37	0.750	0.1160 ± 0.0032	5.4356 ± 0.1469	0.3398 ± 0.0049	1896 ± 28	1886 ± 23
NJ56-02B	109.9	251	0.437	0.0660 ± 0.0016	1.1848 ± 0.0292	0.1302 ± 0.0017	805 ± 30	789 ± 10
NJ56-03	84.0	219	0.384	0.1819 ± 0.0036	11.1104 ± 0.2227	0.4430 ± 0.0057	2670 ± 17	2364 ± 25
NJ56-04	276.2	483	0.572	0.0504 ± 0.0018	0.1794 ± 0.0063	0.0258 ± 0.0004		164 ± 2
NJ56-05	257.6	588	0.438	0.0691 ± 0.0042	0.0719 ± 0.0061	0.0107 ± 0.0002		69 ± 1
NJ56-06	115.7	275	0.421	0.0561 ± 0.0017	0.5358 ± 0.0160	0.0692 ± 0.0009		431 ± 6
NJ56-07	272.6	926	0.294	0.0516 ± 0.0013	0.3000 ± 0.0077	0.0421 ± 0.0006		266 ± 3
NJ56-08	94.0	260	0.362	0.0911 ± 0.0019	3.0720 ± 0.0666	0.2445 ± 0.0032	1449 ± 22	1410 ± 16
NJ56-09	239.2	484	0.494	0.0602 ± 0.0035	0.0630 ± 0.0047	0.0110 ± 0.0002		64 ± 1
NJ56-10	858.9	971	0.885	0.0504 ± 0.0016	0.1258 ± 0.0040	0.0181 ± 0.0003		116 ± 2
NJ56-11	299.0	426	0.702	0.0514 ± 0.0045	0.1308 ± 0.0113	0.0184 ± 0.0003		118 ± 2
NJ56-12B	330.4	466	0.709	0.0557 ± 0.0014	0.5512 ± 0.0143	0.0718 ± 0.0010		447 ± 6
NJ56-13B	174.5	227	0.770	0.0551 ± 0.0020	0.3848 ± 0.0138	0.0506 ± 0.0007		318 ± 4
NJ56-14	669.4	542	1.234	0.0504 ± 0.0020	0.1264 ± 0.0050	0.0182 ± 0.0003		116 ± 2
NJ56-15	260.1	473	0.550	0.0497 ± 0.0018	0.1728 ± 0.0063	0.0252 ± 0.0004		160 ± 2
NJ56-16	206.4	370	0.557	0.1697 ± 0.0034	11.4550 ± 0.2324	0.4894 ± 0.0063	2555 ± 18	2568 ± 27
NJ56-17B	185.0	273	0.677	0.0522 ± 0.0020	0.2698 ± 0.0104	0.0375 ± 0.0005		237 ± 3
NJ56-18B	145.0	205	0.707	0.0538 ± 0.0028	0.1887 ± 0.0097	0.0255 ± 0.0004		162 ± 3
NJ56-19	46.7	461	0.101	0.0539 ± 0.0019	0.4385 ± 0.0144	0.0590 ± 0.0008		369 ± 5
NJ56-20B	404.9	887	0.456	0.0490 ± 0.0014	0.2151 ± 0.0061	0.0319 ± 0.0004		202 ± 3
NJ56-22	135.7	293	0.464	0.0461 ± 0.0028	0.1113 ± 0.0066	0.0175 ± 0.0003		112 ± 2
NJ56-23	447.1	737	0.606	0.0503 ± 0.0014	0.3087 ± 0.0084	0.0445 ± 0.0006		281 ± 4
NJ56-24	220.8	278	0.796	0.0555 ± 0.0029	0.1419 ± 0.0072	0.0185 ± 0.0003		118 ± 2
NJ56-25	225.5	539	0.418	0.1137 ± 0.0024	4.9192 ± 0.1041	0.3137 ± 0.0040	1859 ± 21	1759 ± 20
NJ56-26	320.6	311	1.031	0.0510 ± 0.0026	0.1303 ± 0.0065	0.0185 ± 0.0003		118 ± 2
NJ56-27	454.9	418	1.090	0.0518 ± 0.0020	0.1773 ± 0.0069	0.0248 ± 0.0004		158 ± 2
NJ56-28	943.3	901	1.046	0.0577 ± 0.0015	0.3128 ± 0.0082	0.0393 ± 0.0005		249 ± 3
NJ56-29	176.9	281	0.630	0.0524 ± 0.0020	0.2808 ± 0.0106	0.0389 ± 0.0006		246 ± 3
NJ56-30	148.9	220	0.676	0.0899 ± 0.0021	3.1526 ± 0.0739	0.2543 ± 0.0034	1424 ± 25	1460 ± 17
NJ56-31	702.1	701	1.001	0.0545 ± 0.0020	0.2301 ± 0.0085	0.0306 ± 0.0005		195 ± 3
NJ56-32	84.9	184	0.461	0.0532 ± 0.0027	0.2667 ± 0.0134	0.0363 ± 0.0006		230 ± 4
NJ56-33	156.9	215	0.731	0.0408 ± 0.0032	0.1103 ± 0.0085	0.0196 ± 0.0004		125 ± 2
NJ56-34	507.5	582	0.872	0.0535 ± 0.0016	0.3374 ± 0.0099	0.0458 ± 0.0006		288 ± 4
NJ56-35	257.6	373	0.691	0.0529 ± 0.0023	0.1838 ± 0.0077	0.0252 ± 0.0004		160 ± 2
NJ56-36	226.4	504	0.449	0.0539 ± 0.0038	0.1831 ± 0.0125	0.0246 ± 0.0004		157 ± 3
NJ56-37	118.3	215	0.550	0.0515 ± 0.0021	0.3404 ± 0.0137	0.0479 ± 0.0007		302 ± 4
NJ56-38	2966.9	1829	1.622	0.0527 ± 0.0016	0.2229 ± 0.0066	0.0307 ± 0.0004		195 ± 3
NJ56-39	872.5	495	1.761	0.0509 ± 0.0022	0.1269 ± 0.0054	0.0181 ± 0.0003		116 ± 2
NJ56-40	98.9	221	0.447	0.0959 ± 0.0036	2.9538 ± 0.1039	0.2234 ± 0.0031	1545 ± 73	1300 ± 17
NJ56-41	3780.4	1511	2.502	0.0508 ± 0.0017	0.0903 ± 0.0030	0.0129 ± 0.0002		83 ± 1
NJ56-42	279.1	436	0.640	0.0501 ± 0.0018	0.2407 ± 0.0086	0.0348 ± 0.0005		221 ± 3
NJ56-43	143.7	245	0.587	0.0564 ± 0.0029	0.2017 ± 0.0101	0.0259 ± 0.0004		165 ± 3
NJ56-44	2906.2	1243	2.337	0.0488 ± 0.0015	0.1687 ± 0.0051	0.0250 ± 0.0003		159 ± 2
NJ56-45	91.8	807	0.114	0.1130 ± 0.0031	3.9834 ± 0.0941	0.2556 ± 0.0033	1848 ± 50	1467 ± 17
NJ56-46	438.4	331	1.326	0.0476 ± 0.0047	0.1129 ± 0.0109	0.0172 ± 0.0003		110 ± 2
NJ56-48	132.1	423	0.312	0.0575 ± 0.0017	0.5690 ± 0.0171	0.0718 ± 0.0010		447 ± 6
NJ56-50	218.9	327	0.670	0.0506 ± 0.0019	0.3304 ± 0.0120	0.0474 ± 0.0007		299 ± 4
NJ56-52	137.2	218	0.629	0.0507 ± 0.0026	0.2212 ± 0.0110	0.0317 ± 0.0005		201 ± 3
NJ56-53	84.8	769	0.110	0.0560 ± 0.0020	0.5223 ± 0.0167	0.0677 ± 0.0009		422 ± 6
NJ56-54	741.0	1041	0.712	0.0522 ± 0.0015	0.3504 ± 0.0101	0.0487 ± 0.0007		307 ± 4
NJ56-55	208.8	241	0.865	0.0496 ± 0.0024	0.2268 ± 0.0109	0.0332 ± 0.0005		210 ± 3
NJ56-56	167.6	373	0.449	0.0567 ± 0.0018	0.6237 ± 0.0197	0.0798 ± 0.0011		495 ± 7
NJ56-57	476.4	1060	0.449	0.0562 ± 0.0016	0.5897 ± 0.0163	0.0761 ± 0.0010		473 ± 6
NJ56-58	525.8	336	1.567	0.0537 ± 0.0022	0.2666 ± 0.0108	0.0360 ± 0.0006		228 ± 3
NJ56-59	137.9	395	0.349	0.0545 ± 0.0031	0.1679 ± 0.0092	0.0223 ± 0.0004		142 ± 2
NJ56-60	1359.2	2604	0.522	0.0507 ± 0.0014	0.2627 ± 0.0073	0.0376 ± 0.0005		238 ± 3

All errors are 1 sigma of standard deviation.

### 7.3. Crustal thickening at ~53–22 Ma

The detrital core ages of zircons from the three pelitic gneisses are consistent with Phanerozoic magmatic events within the Gongshan block. Twenty-eight detrital zircon cores with Jurassic to Cretaceous ages (165–64 Ma) are of clear magmatic origin; they have high Th/U

ratios, concordant ages and CL images of oscillatory crystallization, as are zircons from the Gaoligongshan magmatic belt. All the above observations demonstrate that protoliths of the high-grade metamorphic rocks of Gaoligong Group must have been sourced locally and deposited later than the Cretaceous Gaoligongshan magmatic belt. Therefore, we conclude that the Gaoligong Group was most probably

**Table 4**  
U–Th–Pb SHRIMP zircon data of various granites (NJ66 and ST122) within the high-grade metamorphic rocks.

Spot	U ppm	Th ppm	Th/U	Comm	<sup>206</sup> Pb% <sup>b</sup>	<sup>206</sup> Pb* ppm	<sup>206</sup> Pb*/ <sup>238</sup> U	<sup>207</sup> Pb*/ <sup>206</sup> Pb*	<sup>207</sup> Pb*/ <sup>235</sup> U	<sup>206</sup> Pb/ <sup>238</sup> U age (Ma)
<i>Leucogranite (NJ66)</i>										
NJ66-1.1	4076	42	0.011	0.97		19.0	0.0054 ± 0.00008	0.0493 ± 0.0015	0.037 ± 0.0013	34.6 ± 0.5
NJ66-3.1C	4221	98	0.024	1.02		25.5	0.0070 ± 0.00011	0.0464 ± 0.0029	0.045 ± 0.0029	44.8 ± 0.7
NJ66-3.2	3886	26	0.007	2.00		11.9	0.0036 ± 0.00007	0.0386 ± 0.0076	0.022 ± 0.0043	22.6 ± 0.5
NJ66-4.1C	4498	67	0.015	0.99		32.3	0.0083 ± 0.00013	0.0470 ± 0.0020	0.054 ± 0.0024	53.2 ± 0.9
NJ66-4.2	4181	39	0.010	0.90		12.9	0.0035 ± 0.00007	0.0454 ± 0.0096	0.022 ± 0.0047	22.8 ± 0.5
NJ66-5.1	5015	65	0.013	1.62		16.1	0.0037 ± 0.00006	0.0452 ± 0.0051	0.023 ± 0.0026	23.6 ± 0.4
NJ66-6.1	3169	24	0.008	0.92		13.7	0.0050 ± 0.00008	0.0440 ± 0.0021	0.030 ± 0.0015	31.9 ± 0.5
NJ66-7.1	4037	29	0.007	1.93		12.2	0.0034 ± 0.00006	0.0426 ± 0.0048	0.020 ± 0.0023	22.0 ± 0.4
NJ66-8.1	3458	29	0.009	2.08		10.8	0.0035 ± 0.00008	0.0458 ± 0.0092	0.022 ± 0.0045	22.8 ± 0.6
<i>Tourmaline granite (ST122) in the Gongshan block</i>										
ST122-1.1	2363	251	0.11	2.30		8.6	0.0041 ± 0.0002	0.0415 ± 0.0049	0.02 ± 0.003	26.5 ± 1.3
ST122-2.1	2180	244	0.12	2.32		7.9	0.0041 ± 0.0002	0.0446 ± 0.0052	0.03 ± 0.003	26.5 ± 1.3
ST122-3.1	1827	340	0.19	2.22		6.3	0.0039 ± 0.0002	0.0541 ± 0.0077	0.03 ± 0.004	25.2 ± 1.4
ST122-4.1	4469	572	0.13	1.46		13.9	0.0036 ± 0.0001	0.0467 ± 0.0021	0.02 ± 0.001	23.0 ± 0.9
ST122-5.1	21563	1430	0.07	0.33		71.8	0.0039 ± 0.0001	0.0467 ± 0.0017	0.02 ± 0.001	24.8 ± 0.5
ST122-6.1	13927	620	0.05	0.38		50.2	0.0042 ± 0.0001	0.0474 ± 0.0010	0.03 ± 0.001	26.9 ± 0.7
ST122-7.1	4530	493	0.11	1.62		14.9	0.0038 ± 0.0001	0.0476 ± 0.0056	0.02 ± 0.003	24.3 ± 1.0
ST122-8.1	6918	1347	0.20	1.24		21.8	0.0036 ± 0.0001	0.0431 ± 0.0044	0.02 ± 0.002	23.3 ± 1.0
ST122-9.1	3935	233	0.06	2.78		11.9	0.0034 ± 0.0001	0.0458 ± 0.0026	0.02 ± 0.001	22.8 ± 1.0
ST122-10.1	7937	1892	0.25	0.81		25.2	0.0037 ± 0.0001	0.0471 ± 0.0044	0.02 ± 0.002	23.6 ± 0.7
ST122-11.1	17145	2666	0.16	0.57		61.5	0.0042 ± 0.0001	0.0428 ± 0.0009	0.02 ± 0.001	26.7 ± 0.9
ST122-12.1	12863	621	0.05	0.41		42.9	0.0039 ± 0.0001	0.0468 ± 0.0014	0.02 ± 0.001	24.9 ± 0.5

All errors are 1 sigma of standard deviation. C = core.  
Pb\* is the radiogenic lead.

deposited during the India–Asia collision in the Paleocene (~65–55 Ma) (e.g., Yin and Harrison, 2000).

Medium to high-pressure granulite-facies metamorphic rocks of Paleogene sediments in the southern Gongshan block (this study) and in the Baoshan Block (YBGMR, 1990; Zhai et al., 1990; Zhong, 1998), and high-pressure granulite ( $T = 750\text{--}860\text{ }^{\circ}\text{C}$  and  $P = 8\text{--}10\text{ kbar}$ ) at 23–24 Ma in the Tengchong block (Ji et al., 2000b) indicate a regional high  $P$ – $T$  metamorphic event. Compositional zonation of garnet suggests a  $P$ – $T$  reflects prograde metamorphic event, which we interpret as indicating crustal thickening that buried the Paleogene sediments to depths of ~24–30 km prior to ~22 Ma. The ~53–22 Ma magmatism of crustal melting (samples NJ66, NJ74 and ST122), as well as high-grade metamorphism, suggests that the duration of crustal thickening may be ~30 m.y. Occurrence of the high-grade metamorphic rocks and leucogranites suggests that they must have resulted from regional metamorphism prior to ~22 Ma rather than associated with spatially restricted narrow lateral-slip shear zones (see below). Microstructural

analyses show that the mylonite formed by right-lateral slip is a later low-grade metamorphic event (see above), and overprints the earlier high-grade regional metamorphism.

High-grade metamorphic rocks and leucogranites of ~35 Ma to ~17 Ma along the Ailaoshan–Red River fault zone have been interpreted as a result of strike-slip deformation (Schärer et al., 1990, 1994; Harrison et al., 1992; Leloup et al., 1995, 2001; Zhang and Schärer, 1999; Gilley et al., 2003). However, Searle (2006) pointed out that mylonites along the Red River Fault with left-slip kinematic indicators are also lower-temperature fabrics formed after peak sillimanite metamorphism, suggesting that the left-lateral strike-slip shearing along the Red River fault started after ~21 Ma.

Boitite and muscovite K–Ar and <sup>40</sup>Ar–<sup>39</sup>Ar ages from the Gaoligong mylonitic shear zone range from 32 Ma to 11 Ma (Wang and Burchfiel, 1997; Ji et al., 2000a; Wang et al., 2006), which is interpreted as representing the duration of fault movement. Although this shear zone displays characteristics of right-lateral slip, it is petrographically

**Table 5**  
U–Th–Pb LA–ICP–MS zircon data of the tourmaline-bearing granite NJ74.

Analysis	Th ppm	U ppm	Th/U	<sup>207</sup> Pb/ <sup>206</sup> Pb	<sup>207</sup> Pb/ <sup>235</sup> U	<sup>206</sup> Pb/ <sup>238</sup> U	<sup>207</sup> Pb/ <sup>206</sup> Pb age (Ma)	<sup>206</sup> Pb/ <sup>238</sup> U age (Ma)
NJ74-01	75	871	0.086	0.0519 ± 0.0053	0.0234 ± 0.0024	0.00374 ± 0.00009		24.2 ± 0.6
NJ74-02	59	1217	0.049	0.0511 ± 0.0028	0.0281 ± 0.0015	0.00400 ± 0.00009		25.7 ± 0.6
NJ74-03	51	842	0.061	0.0429 ± 0.0039	0.0232 ± 0.0019	0.00389 ± 0.00009		25.1 ± 0.6
NJ74-04	113	1264	0.090	0.0465 ± 0.0021	0.0342 ± 0.0015	0.00533 ± 0.00010		34.3 ± 0.7
NJ74-05	60	856	0.070	0.0477 ± 0.0047	0.0257 ± 0.0025	0.00391 ± 0.00011		25.2 ± 0.7
NJ74-06	66	1059	0.062	0.0512 ± 0.0052	0.0257 ± 0.0030	0.00423 ± 0.00013		27.2 ± 0.7
NJ74-07	228	1593	0.143	0.0501 ± 0.0033	0.0258 ± 0.0020	0.00405 ± 0.00011		26.1 ± 0.7
NJ74-08	75	728	0.103	0.0461 ± 0.0014	0.0257 ± 0.0006	0.00404 ± 0.00011		26.0 ± 0.7
NJ74-09	291	1606	0.181	0.0497 ± 0.0027	0.0397 ± 0.0021	0.00579 ± 0.00013		37.2 ± 0.9
NJ74-10	641	1793	0.357	0.0461 ± 0.0026	0.0382 ± 0.0021	0.00602 ± 0.00013		38.7 ± 0.9
NJ74-11	1378	2658	0.518	0.0533 ± 0.0020	0.0415 ± 0.0018	0.00646 ± 0.00014		41.5 ± 0.9
NJ74-12	42	1086	0.039	0.0430 ± 0.0031	0.0235 ± 0.0016	0.00380 ± 0.00010		24.4 ± 0.6
NJ74-13	56	1141	0.049	0.0487 ± 0.0032	0.0266 ± 0.0017	0.00397 ± 0.00010		25.5 ± 0.6
NJ74-14	1084	11116	0.098	0.0457 ± 0.0017	0.0237 ± 0.0007	0.00400 ± 0.00006		25.7 ± 0.4
NJ74-15	43	826	0.052	0.0387 ± 0.0033	0.0237 ± 0.0020	0.00381 ± 0.00011		25.5 ± 0.7
NJ74-16	402	1012	0.398	0.0486 ± 0.0062	0.0375 ± 0.0047	0.00560 ± 0.00014		36.0 ± 0.9
NJ74-17	36	45	0.787	0.1599 ± 0.0052	9.9500 ± 0.3220	0.45113 ± 0.00691	2455 ± 34	2400 ± 31
NJ74-18	57	1355	0.042	0.0453 ± 0.0027	0.0250 ± 0.0015	0.00400 ± 0.00010		25.7 ± 0.6

All errors are 1 sigma of standard deviation.

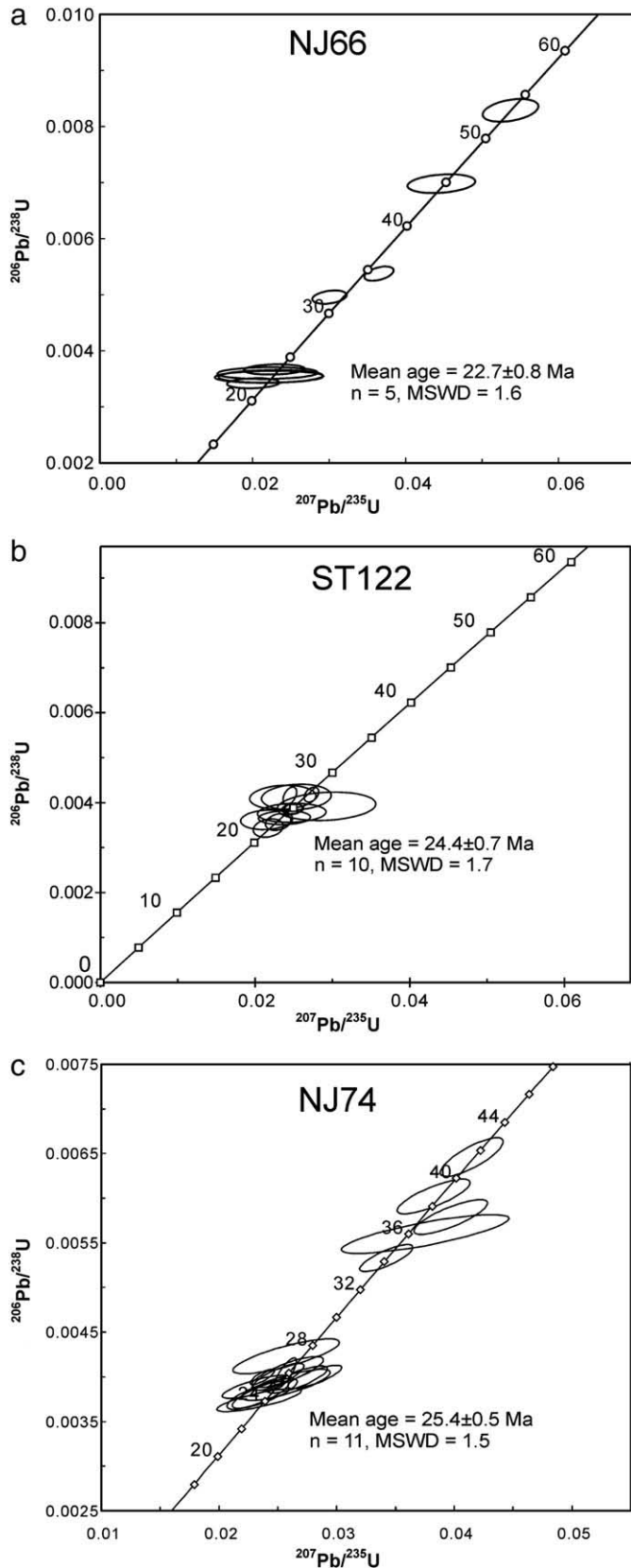


**Fig. 11.** Concordia diagrams and histogram of apparent  $^{206}\text{Pb}/^{238}\text{U}$  ages for zircons from (a) the leucogranite (NJ66), (b) and (c) the tourmaline granite (ST122 and NJ74).

apparent that these deformational features are rather late. Note that most biotite and amphibole for Ar–Ar dating, as described by Ji et al. (2000a,b) and Wang et al. (2006), are deformed porphyroclasts in

mylonites, similar to those described above in Figs. 2 and 4. Petrographically, they are apparently generated by regional orogenic metamorphism prior to mylonization, and thus cannot represent ages of strike-slip shear zones. The Sagaing Fault, the west boundary fault of the Indochina continent, was active no earlier than 15 m.y. (Morley et al., 2001; Replumaz and Tapponnier, 2003), which places a constraint on the timing and scale of southeastward extrusion. In this context, it is important to note that there is no experimental proof that strike-slip shearing is an effective mechanism to cause anatexis and granitoid magmatism. All these observations and reasoning support our interpretation that the pre-22 Ma tectonism in this region was mostly predominated by vertical thickening.

The Gaoligong shear zone is only an internal fault within the NIC. Granitoid intrusions along the Gaoligongshan magmatic belt, as well as the Paleozoic strata, are cut and deformed by the Gaoligong shear zone and by later brittle faults without significant displacement (see Fig. 1b). The intense isoclinal folding and the development of vertical axial-plane schistosity with the accompanied regional medium- to high-grade metamorphism (Fig. 4) are strong evidence for crustal shortening and thickening as a result of the persistent northward compression of the Indian Plate. Such strong crustal shortening explains (1) clockwise rotation of Indochina around the Eastern Himalayan Syntaxis as revealed by the Tertiary paleomagnetic data from the northwestern Yunnan (Sato et al., 2001), which continues to the present as shown by the GPS data (e.g., Wang et al., 2004); (2) rapid underthrusting (Paleocene sediments down to depths of 25–30 km at ~22 Ma), high-grade metamorphism and related anatexis before ultimate exhumation to the surface in the NIC region; and (3) separation of the Indochina continent from the Lhasa Block around the Eastern Himalayan Syntaxis.

## 8. Conclusion

- (1) The northern Indochina continent (NIC, including the Gongshan, Tengchong, and Baoshan blocks) near the Eastern Himalayan Syntaxis has the affinity with the Lhasa Block in southern Tibet. They may possess the same early Precambrian basement and have shared the same or similar multiple granitic magmatic events from the Neoproterozoic, early Paleozoic, Triassic, Cretaceous, and to the Cenozoic.
- (2) Continued northeastward convergence of the Indian Plate led to significant crustal thickening in the NIC during the period of ~53–22 Ma, which involved rapid underthrusting of the Paleocene to Eocene sediments to depths of 25–30 km. Deep crustal high-grade metamorphism and anatexis produced the present-day observed metamorphic rocks and granitic intrusions in the NIC.
- (3) Continued northeastward convergence of the Indian Plate and the resistance at the Eastern Himalayan Syntaxis resulted in the clockwise rotation and physical separation of the Indochina continent from the Lhasa Block.
- (4) Gaoligongshan magmatic belt is the southern/eastern continuation of the Gangdese magmatic belt although the magmatism continued independently in the past ~30 m.y. since their separation.

Supplementary materials related to this article can be found online at [doi:10.1016/j.lithos.2010.08.021](https://doi.org/10.1016/j.lithos.2010.08.021).

## Acknowledgements

We thank B. Song and D.Y. Liu for help in the SHRIMP lab work, and E. Kirby for constructive comments on an early version of the manuscript. We also thank G.C. Zhao, Y.B. Wang and I. Buick for their detailed and rather constructive review comments, which led to a

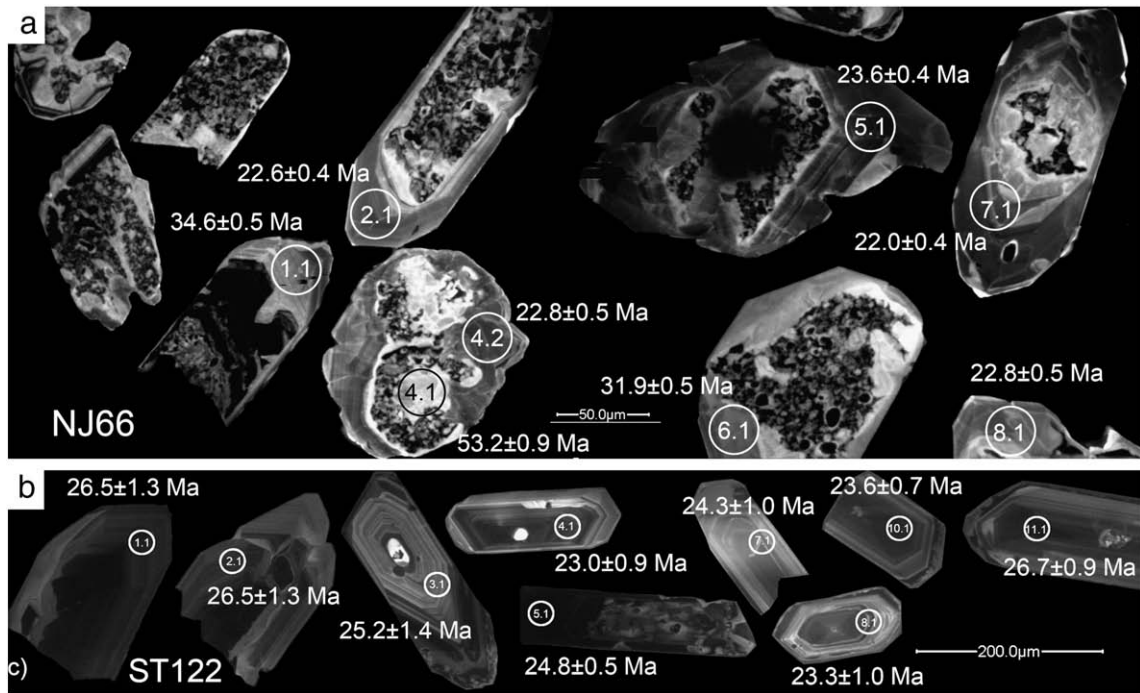


Fig. 12. Representative CL images for zircons from Cenozoic granite in the southern segment of the Gongshan block. (a) Leucogranite NJ66; and (b) tourmaline granite ST122.

better presentation of the final product. This study was financially supported by Chinese National Natural Science Foundation (grants nos. 40825007, 40821002), the Foundation for the Author of National Excellent Doctoral Dissertation of China (200531), and the Royal Society International Fellowship provided by the K C Wong Education Foundation awarded to Shuguang Song.

## References

- Andersen, T., 2002. Correction of common lead in U-Pb analyses that do not report  $^{204}\text{Pb}$ . *Chemical Geology* 192, 59–79.
- Avigad, D., Kolodner, K., McWilliams, M., Persing, H., Weissbrod, T., 2003. Origin of northern gondwana Cambrian sandstone revealed by detrital zircon SHRIMP dating. *Geology* 31, 227–230.

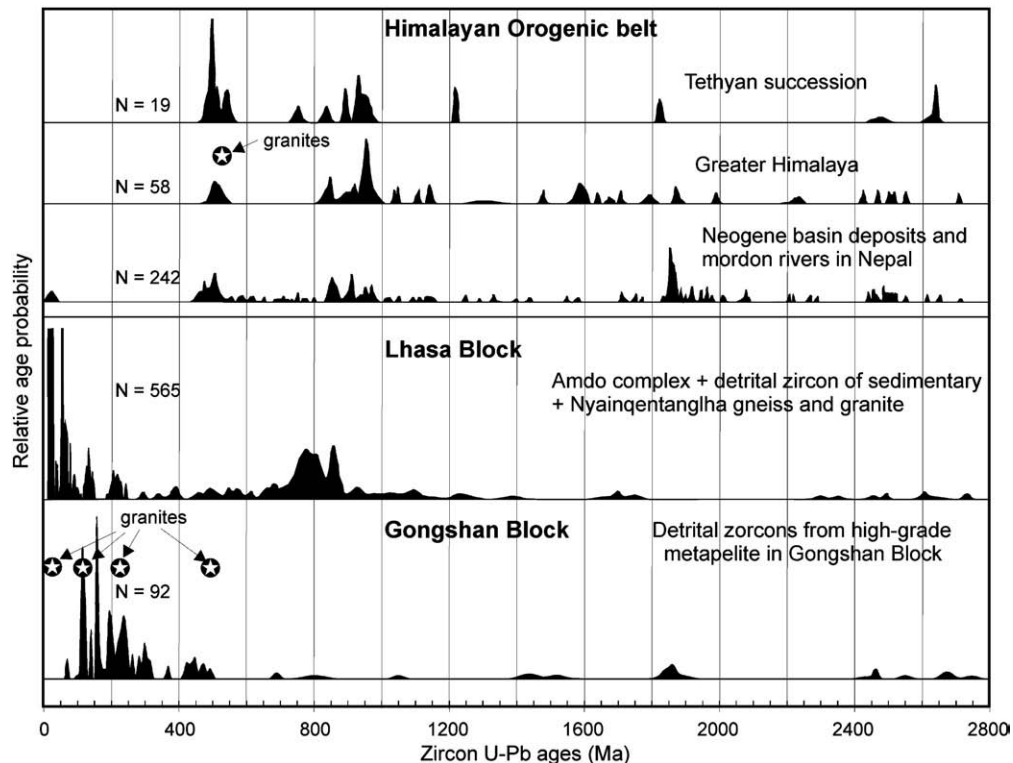


Fig. 13. Comparison of zircon U-Pb age spectra on samples from the Himalayan Orogenic Belt (DeCelles et al., 2000), Lhasa Block (Hu et al., 2004; Kapp et al., 2005a,b; Guynn et al., 2006; Yang and Li, 2006; Duo et al., 2007) and Gongshan block of the NIC. Stars with black circles indicate intrusive bodies.

- Bertrand, G., Rangin, C., Maluski, H., Han, T.A., Thein, M., Myint, O., Maw, W., Lwin, S., 1999. Cenozoic metamorphism along the Shan scarp (Myanmar): evidences for ductile shear along the Sagaing fault or the northward migration of the eastern Himalayan syntaxis. *Geophysical Research Letters* 26, 915–918.
- Bertrand, G., Rangin, C., Maluski, H., Bellon, H., 2001. Diachronous cooling along the Mogok metamorphic belt (Shan scarp, Myanmar): the trace of the northward migration of the Indian syntaxis. *Journal of Asian Earth Sciences* 19, 649–659.
- Black, L.P., Kamo, S.L., Allen, C.M., Aleinikoff, J.N., Davis, D.W., Korsch, R.J., Foudoulis, C., 2003. TEMORA 1: a new zircon standard for Phanerozoic U–Pb geochronology. *Chemical Geology* 200, 155–170.
- Bodet, F., Schärer, U., 2000. Evolution of the SE-Asian continent from U–Pb and Hf isotopes in single grains of zircon and baddeleyite from large rivers. *Geochimica Et Cosmochimica Acta* 64, 2067–2091.
- Burchfiel, B.C., Wang, E., 2003. Northwest-trending, middle Cenozoic, left-lateral faults in southern Yunnan, China, and their tectonic significance. *Journal of Structure Geology* 25, 781–792.
- Carter, A., Roques, D., Bristow, C., Kinny, P., 2001. Understanding Mesozoic accretion in Southeast Asia: significance of Triassic thermotectonism (Indosinian orogeny) in Vietnam. *Geology* 29, 211–214.
- Chen, J.F., Jahn, B.M., 1998. Crustal evolution of southeastern China: Nd and Sr isotopic evidence. *Tectonophysics* 284, 101–133.
- Chen, F.K., Siebel, W., Guo, J.H., 2004. Zircon age evidence for Early Paleozoic magmatism in the Baoshan-Tengchong block of the Tethyan Yunnan, China. 2004 Goldschmidt Conference, Copenhagen, Denmark. A547.
- Chen, Y.L., Luo, Z.H., Zhao, J.X., Li, Z.H., Zhang, H.F., Song, B., 2005. Petrogenesis and dating of the Kangding complex, Sichuan Province. *Acta Geologica Sinica-English Edition* 48, 622–634.
- Chen, F.K., Li, Q.L., Wang, X.L., Li, X.H., 2006. Zircon age and Sr–Nd–Hf isotopic composition of migmatite in the eastern Tengchong block, western Yunnan. *Acta Petrologica Sinica* 22, 439–448.
- Chu, M.F., Chung, S.L., Song, B., Liu, D.Y., O'Reilly, S.Y., Pearson, N.J., Ji, J.Q., Wen, D.J., 2006. Zircon U–Pb and Hf isotope constraints on the Mesozoic tectonics and crustal evolution of southern Tibet. *Geology* 34, 745–748.
- Compston, W., Williams, I.S., Kirschvink, J.L., Zhang, Z., Ma, G., 1992. Zircon U–Pb ages for the Early Cambrian time-scale. *Journal of the Geological Society of London* 149, 171–184.
- DeCelles, P.G., Gehrels, G.E., Quade, J., LaReau, B., Spurlin, M., 2000. Tectonic implications of U–Pb zircon ages of the Himalayan orogenic belt in Nepal. *Science* 288, 497–499.
- Duo, J., Wen, C.Q., Guo, J.C., Fan, X.P., Li, X.W., 2007. 4.1 Ga old detrital zircon in western Tibet of China. *Chinese Science Bulletin* 52, 23–26.
- England, P., Molnar, P., 1990. Right-lateral shear and rotation as the explanation for strike-slip faulting in eastern Tibet. *Nature* 344, 140–142.
- England, P.C., Molnar, P., 1997. The field of crustal velocity in Asia calculated from Quaternary rates of slip on faults. *Geophysical Journal International* 130, 551–582.
- England, P., Molnar, P., 2005. Late Quaternary to decadal velocity fields in Asia. *Journal of Geophysical Research, Solid Earth* 110 (B12).
- Gilley, L.D., Harrison, T.M., Leloup, P.H., Ryerson, F.J., Lovera, O.M., Wang, J.-H., 2003. Direct dating of left-lateral deformation along the Red River shear zone, China and Vietnam. *Journal of Geophysical Research* 108 (B2), 2127. doi:10.1029/2001JB001726.
- Gyynn, J.H., Kapp, P., Pullen, A., Heizler, M., Gehrels, G., Ding, L., 2006. Tibetan basement rocks near Amdo reveal “missing” Mesozoic tectonism along the Bangong suture, central Tibet. *Geology* 34, 505–508.
- Hanson, R.E., Crowley, J.L., Bowring, S.A., Ramezani, J., Gose, W.A., Dalziel, I.W.D., Pancake, J.A., Seidel, E.K., Blenkinsop, T.G., Mukwakwami, J., 2004. Coeval large-scale magmatism in the Kalahari and Laurentian Cratons during Rodinia assembly. *Science* 304, 1126–1129.
- Harrison, T.M., Chen, W., Leloup, P.H., Ryerson, F.J., Tapponnier, P., 1992. An Early Miocene transition in deformation regime within the Red River fault zone, Yunnan, and its significance for Indo-Asian tectonics. *Journal of Geophysical Research* 97, 7159–7182.
- Hoffman, P.F., Kaufman, A.J., Halverson, G.P., Schrag, D.P., 1998. A Neoproterozoic snowball Earth. *Science* 281, 1342–1346.
- Holdaway, M.J., 2000. Application of new experimental and garnet Margules data to the garnet-biotite geothermometer. *American Mineralogist* 85, 881–892.
- Holland, T.J.B., Powell, R., 1998. An internally consistent thermodynamic data set for phases of petrological interest. *Journal of Metamorphic Geology* 16, 309–343.
- Holt, W.E., Ni, J.F., Wallace, T.C., 1991. The active tectonics of the eastern Himalayan Syntaxis and surrounding regions. *Journal of Geophysical Research* 96, 14595–14632.
- Houseman, G., England, P., 1993. Crustal thickening versus lateral expulsion in the Indian–Asian continental collision. *Journal of Geophysical Research* 98, 12233–12249.
- Hu, D.G., Wu, Z.H., Jiang, W., Shi, Y.R., Ye, P.S., Liu, Q.S., 2004. SHRIMP zircon U–Pb age and Nd isotopic study on the Nyainqentanglha Group in Tibet. *Chinese Science Bulletin* 49, 76–82.
- Ji, J.Q., Zhong, D.L., Sang, H.Q., Zhang, L.S., 2000a. The western boundary of extrusion blocks in the southeastern Tibetan Plateau. *Chinese Science Bulletin* 45, 876–881.
- Ji, J.Q., Zhong, D.L., Shang, H.Q., Qiu, J., Hu, S.L., 2000b. Dating of two metamorphic events on the basalt granulite from the Nabang area on the border of China and Burma. *Acta Petrologica Sinica* 16, 227–232.
- Kapp, J.L.D., Harrison, T.M., Kapp, P., Grove, M., Lovera, O.M., Lin, D., 2005a. Nyainqentanglha Shan: A window into the tectonic, thermal, and geochemical evolution of the Lhasa block, southern Tibet. *Journal of Geophysical Research* 110, B08413.
- Kapp, P., Yin, A., Harrison, T.M., Ding, L., 2005b. Cretaceous–Tertiary shortening, basin development, and volcanism in central Tibet. *Geological Society of America Bulletin* 117, 865–878.
- Lan, C.Y., Chung, S.L., Shen, J.J., Lo, C.H., Wang, P.L., Hoa, T.T., Thanh, H.H., Mertzman, S.A., 2000. Geochemical and Sr–Nd isotopic characteristics of granitic rocks from northern Vietnam. *Journal of Asian Earth Sciences* 18, 267–280.
- Lan, C.Y., Chung, S.L., Lo, C.H., Lee, T.Y., Wang, P.L., Li, H.M., Toan, D.V., 2001. First evidence for Archean continental crust in northern Vietnam and its implications for crustal and tectonic evolution in Southeast Asia. *Geology* 29, 219–222.
- Lee, H.-Y., Chung, S.-L., Wang, J.-R., Wen, D.-J., Lo, C.-H., Yang, T.F., Zhang, Y., Xie, Y., Lee, T.-Y., Wu, G.Y., Ji, J.Q., 2003. Miocene Jiali faulting and its implications for Tibetan tectonic evolution. *Earth and Planetary Science Letters* 205, 185–194.
- Leloup, P.H., Cacassin, R., Tapponnier, P., Schärer, U., Zhong, D., Liu, X., Zhang, L., Ji, S., Trinh, P.T., 1995. The Ailao Shan–Red River shear zone (Yunnan, China), Tertiary transform boundary of Indochina. *Tectonophysics* 251, 3–84.
- Leloup, H.P., Arnaud, N., Lacassin, R., Kienast, J.R., Harrison, T.M., Trinh, P.T., Replumaz, A., Tapponnier, P., 2001. New constraints on the structure, thermochronology and timing of the Ailao Shan–Red River shear zone, SE Asia. *Journal of Geophysical Research* 106, 6683–6732.
- Li, Z.X., Li, X.H., Kinny, P.D., Wang, J., 1999. The breakup of Rodinia: did it start with a mantle plume beneath South China? *Earth and Planetary Science Letters* 173, 171–181.
- Li, Z.X., Li, X.H., Kinny, P.D., Wang, J., Zhang, S., Zhou, H., 2003. Geochronology of Neoproterozoic syn-rift magmatism in the Yangtze Craton, South China and correlations with other continents: evidence for a mantle superplume that broke up Rodinia. *Precambrian Research* 122, 85–109.
- Ludwig, K.R., 2003. User's Manual for Isoplot 3.0: A Geochronological Toolkit for Microsoft Excel Berkeley Geochronology Center, vol. 4, pp. 1–71. special publication.
- Mitchell, A.H.G., 1989. The Shan Plateau and Western Burma: Mesozoic–Cenozoic plate boundaries and correlations with Tibet. In: Sengor, A.M.C. (Ed.), *Tectonic Evolution of the Tethyan Region*. Kluwer Academic Publications, Paris, pp. 567–583.
- Morley, C.K., Woganan, N., Sankumarn, N., Hoon, T.B., Alief, A., Simmons, M., 2001. Late Oligocene–Recent stress evolution in rift basins of Northern and Central Thailand: implications for escape tectonics. *Tectonophysics* 334, 115–150.
- Pan, G.T., Ding, J., 2004. Geologic map of the Tibetan Plateau and adjacent areas (scale 1:1500000). Chengdu Cartographic Publishing House.
- Peltzer, G., Tapponnier, P., 1988. Formation and evolution of strike-slip faults, rifts, and basins during the India–Asia collision: an experimental approach. *Journal of Geophysical Research* 93, 15085–15117.
- Peng, T.P., Wang, Y.J., Fan, W.M., Liu, D.Y., Shi, Y.R., Miao, L.C., 2006. SHRIMP zircon U–Pb geochronology of early Mesozoic felsic igneous rocks from the southern Lancangjiang and its tectonic implications. *Science in China Series D: Earth Sciences* 49, 1032–1042.
- Powell, R., Holland, T., Worley, B., 1998. Calculating phase diagram involving solid solutions via non-linear equations, with examples using THERMOCALC. *Journal of Metamorphic Geology* 16, 577–586.
- Replumaz, A., Tapponnier, P., 2003. Reconstruction of the deformed collision zone between India and Asia by backward motion of lithospheric blocks. *Journal of Geophysical Research* 108 (B6), 2285. doi:10.1029/2001JB000661.
- Rubatto, D., Gebauer, D., Compagnoni, R., 1999. Dating of eclogite-facies zircons: the age of Alpine metamorphism in the Sesia–Lanzo Zone (Western Alps). *Earth and Planetary Science Letters* 167, 141–158.
- Sato, K., Liu, Y.Y., Zhu, Z.C., Yang, Z.Y., Otofujii, Y., 2001. Tertiary paleomagnetic data from northwestern Yunnan, China: further evidence for large clockwise rotation of the Indochina block and its tectonic implications. *Earth and Planetary Science Letters* 185, 185–198.
- Schärer, U., Tapponnier, P., Lacassin, R., Leloup, P.H., Zhong, D., Ji, S., 1990. Intraplate tectonics in Asia: a precise age for large scale Miocene movement along the Ailao Shan–Red River shear zone, China. *Earth and Planetary Science Letters* 97, 65–77.
- Schärer, U., Zhang, L.S., Tapponnier, P., 1994. Duration of strike-slip movements in large shear zones: the Red River belt, China. *Earth and Planetary Science Letters* 126, 379–397.
- Schelling, D., 1992. The tectonostratigraphy and structure of the Eastern Nepal Himalaya. *Tectonics* 11, 925–943.
- Searle, M.P., 2006. Role of the Red River Shear zone, Yunnan and Vietnam, in the continental extrusion of SE Asia. *Journal of the Geological Society of London* 163, 1025–1036.
- Socquet, A., Pubellier, M., 2005. Cenozoic deformation in western Yunnan (China–Myanmar border). *Journal of Asian Earth Sciences* 24, 495–515.
- Song, S.G., Zhang, L.F., Niu, Y., Su, L., Song, B., Liu, D.Y., 2006. Evolution from oceanic subduction to continental collision: a case study from the Northern Tibetan Plateau based on geochemical and geochronological data. *Journal of Petrology* 47, 435–455.
- Song, S.G., Ji, J.Q., Wei, C.J., Su, L., Zheng, Y.D., Song, B., Zhang, L.F., 2007. Early Paleozoic granite in Nujiang River of northwest Yunnan in SW China and its tectonic implications. *Chinese Science Bulletin* 52, 2402–2406.
- Stacey, J.S., Kramers, J.D., 1975. Approximation of terrestrial lead isotope evolution by a two-stage model. *Earth and Planetary Science Letters* 26, 207–221.
- Tapponnier, P., Peltzer, G., Armijo, R., 1986. On the mechanics of the collision between India and Asia. In: Coward, M.P., Ries, A.C. (Eds.), *Collision Tectonics: Geological Society, London*, vol. 19, pp. 115–157. Special Publication.
- Tapponnier, P., Lacassin, R., Leloup, P.H., Schärer, U., Zhong, D.L., Wu, H.W., Liu, X.H., Ji, S.C., Zhang, L.S., Zhong, J.Y., 1990. The Ailao Shan/Red River metamorphic belt: Tertiary left-lateral shear between Indochina and South China. *Nature* 343, 431–437.
- Tapponnier, P., Xu, Z.Q., Roger, F., Meyer, B., Arnaud, N., Wittlinger, G., Yang, J.S., 2001. Geology–oblique stepwise rise and growth of the Tibet plateau. *Science* 294, 1671–1677.
- Vavra, G., Gebauer, D., Schmidt, R., Compston, W., 1996. Multiple zircon growth and recrystallization during polyphase Late Carboniferous to Triassic metamorphism in granulites of the Ivrea Zone (Southern Alps): an ion microprobe (SHRIMP) study. *Contributions to Mineralogy and Petrology* 122, 337–358.

- Wang, Y., 1983. The characteristics and significance of Carboniferous gravel beds in the Tengchong and Baoshan area, western Yunnan. In: Zhou, Z., Xu, X., Zhou, W. (Eds.), *Geology of Qinghai–Xizang (Tibet) Plateau*, Beijing, vol. 11, pp. 71–77.
- Wang, E., Burchfiel, B.C., 1997. Interpretation of Cenozoic tectonics in the right-lateral accommodation zone between the Ailao Shan shear zone and the eastern Himalayan syntaxis. *International Geology Review* 39, 191–219.
- Wang, Q., Zhang, P., Freymueller, J.T., Bilham, R., Larson, K.M., Lai, X., You, X., Niu, Z., Wu, J., Li, Y., Liu, J., Yang, Z., Chen, Q., 2004. Present-day crustal deformation in continental China constrained by Global Positioning System measurements. *Science* 294, 574–577.
- Wang, Y.J., Fan, W.M., Zhang, Y.H., Peng, T.P., Chen, X.Y., Xu, Y.G., 2006. Kinematics and  $^{40}\text{Ar}/^{39}\text{Ar}$  geochronology of the Gaoligong and Chongshan shear systems, western Yunnan, China: implications for early Oligocene tectonic extrusion of SE Asia. *Tectonophysics* 418, 235–254.
- Wiedenbeck, M., Alle, P., Corfu, F., Griffin, W.L., Meier, M., Oberli, F., Vonquadt, A., Roddick, J.C., Speigel, W., 1995. Three natural zircon standards for U–Th–Pb, Lu–Hf, trace-element and REE analyses. *Geostandard Newsletter* 19, 1–23.
- Williams, I.S., 1996. The response of zircon, monazite and their U–Pb isotopic systems, to low-P, high-T regional metamorphism leading to host rock partial melting. *Geological Society of America Abstracts with Programs* 28, A357.
- Williams, I.S., Claesson, S., 1987. Isotopic evidence for the Precambrian provenance and Caledonian metamorphism of high grade paragneisses from the Seve Nappes, Scandinavian Caledonides, II. Ion microprobe zircon U–Th–Pb. *Contributions to Mineralogy and Petrology* 97, 205–217.
- Xu, R.H., Schärer, U., Allègre, C.J., 1985. Magmatism and metamorphism in the Lhasa block (Tibet): a geochronological study. *Journal of Geology* 93, 41–57.
- Yan, C.M., Xia, G.G., Deng, R.H., 2002. Characteristics of Dulongjiang granite and magmatism in Northwest Yunnan. *Yunnan Geology* 21, 21–33 (in Chinese with English abstract).
- Yang, Z.J., Li, X.Y., 2006. SHRIMP U–Pb dating of zircons from low-grade metamorphic rocks in the Rola Kangri junction zone, northern Tibet, China. *Geological Bulletin of China* 25, 118–123.
- YBGMR (Yunnan Bureau of Geology and Mineral Resources), 1990. *Regional Geology of the Yunnan Province*. Geological Publishing House, Beijing. 592 pp. (in Chinese with English abstract).
- Yin, A., 2006. Cenozoic tectonic evolution of the Himalayan orogen as constrained by along-strike variation of structural geometry, exhumation history, and foreland sedimentation. *Earth Science Reviews* 76, 1–131.
- Yin, A., Harrison, T.M., 2000. Geologic evolution of the Himalayan–Tibetan orogen. *Annual Review of Earth and Planetary Sciences* 28, 211–280.
- Zhai, M.G., Cong, B.L., Qiao, G.S., Zhang, R.Y., 1990. Sm–Nd and Rb–Sr geochronology of metamorphic rocks from SW Yunnan orogenic zones, China. *Acta Petrologica Sinica* 6, 1–11 (in Chinese with English abstract).
- Zhang, L.S., Schärer, U., 1999. Age and origin of magmatism along the Cenozoic Red River shear belt, China. *Contributions to Mineralogy and Petrology* 134, 67–85.
- Zhang, B., Zhang, J.J., Zhong, D.L., 2010. Structure, kinematics and ages of transpression during strain-partitioning in the Chongshan shear zone, western Yunnan, China. *Journal of Structure Geology* 32, 445–463.
- Zhao, J.X., Chen, Y.L., Li, Z.H., 2006. Zircon U–Pb SHRIMP dating for the Kangding Complex and its geological significance. *Geoscience* 20, 378–385 (in Chinese with English abstract).
- Zhong, D., 1998. *Paleo-Tethyan orogenic belt in the western parts of the Sichuan and Yunnan Provinces*. Science Press, Beijing. 231 pp. (in Chinese with English abstract).
- Zhu, D.C., Mo, X.X., Pan, G.T., Zhao, Z.D., Dong, G.C., Shi, Y.R., Liao, Z.L., Wang, L.Q., Zhou, C.Y., 2008. Petrogenesis of the earliest Early Cretaceous mafic rocks from the Cona area of the eastern Tethyan Himalaya in south Tibet: interaction between the incubating Kerguelen plume and the eastern Greater India lithosphere. *Lithos* 100, 147–173.
- Zhu, D.C., Mo, X.X., Niu, Y.L., Zhao, Z.D., Wang, L.Q., Liu, Y.S., Wu, F.Y., 2009. Geochemical investigation of Early Cretaceous igneous rocks along an east-west traverse throughout the central Lhasa Terrane, Tibet. *Chemical Geology* 268, 298–312.